CHALMERS
UNIVERSITY OF TECHNOLOGY

Measurement-Controlled Engines

Investigating the role of system-meter coupling time quantum information engines

Master's thesis in Physics

RASMUS HAGMAN

Department of Microtechnology and Nanoscience
CHALMERS UNIVERSITY OF TECHNOLOGY
Gothenburg, Sweden 2025
www.chalmers.se

Master's thesis 2025

Measurement Controlled Engines

Investigating the role of system-meter correlation time in quantum information engines

Rasmus Hagman

CHALMERS
UNIVERSITY OF TECHNOLOGY

Department of Microtechnology and Nanoscience
Applied Quantum Physics
Dynamics and thermodynamics of nanoscale devices
Chalmers University of Technology
Gothenburg, Sweden 2025

Quantum Information Engine: Converting Information to Useful Work
Investigating the role of system-meter correlation time in quantum information engines
RASMUS HAGMAN

Supervisor: Henning Kirchberg, Department of Microtechnology and Nanoscience, Chalmers University of Technology
Examiner: Janine Splettstösser, Department of Microtechnology and Nanoscience, Chalmers University of Technology

Master's Thesis 2025
Department of Microtchnology and Nanoscience
Applied Quantum Physics
Dynamics and thermodynamics of nanoscale devices
Chalmers University of Technology
SE-412 96 Gothenburg
Telephone +46 31 772 1000

Cover: Image of a demon holding a stopwatch, observing a heat engine, created with the assistance of the Gemini AI model.

Printed by Chalmers Reproservice
Gothenburg, Sweden 2025

Quantum Information Engine: Converting Information to Useful Work
Investigating the role of system-meter correlation time in quantum information engines
RASMUS HAGMAN
Department of Microtchnology and Nanoscience
Chalmers University of Technology

Abstract

Nanoscale devices that transform energy into useful work are becoming ubiquitous. A critical task is to control energy transduction at the nanoscale. In this context, quantum measurement and the associated information acquisition can be leveraged to guide and enhance work output through feedback control. This thesis explores a quantum information engine as a prototype energy-transducing device controlled by measurement. This engine harnesses information transfer between a working medium, modelled as a two-level system, and a meter, modelled as a quantum harmonic oscillator. However, this information transfer is not instantaneous; it depends on the coupling time, which is the time required to correlate the system and the meter. This measurement time sets a lower bound on the cycle time of the quantum information engine, making information acquisition a crucial resource for the process.
We investigate the cost of quantum measurement, in particular the energetic cost of coupling and decoupling the system and the meter in finite-time operations. Furthermore, we analyse possible schemes of extracting useful work: the ergotropy, or maximum work extraction under unitary transformations, and the excess work by stimulated emission. In both cases, the information about the system is exploited by conditioning the act of extracting work on the measurement outcome. Heat and work flows are analysed as functions of the system and meter temperatures to show that the quantum information engine can operate in different regimes: as a heat engine, a heat valve, a refrigerator and a "true" information engine by extracting work and cooling a colder bath. We show that the quantum information engine performance in terms of power output for very short measurement times, the Zeno limit, is small. To increase the power we need to increase the measurement time which, however, comes with a higher cost of measurement. We carefully analyse the work output-cost relation in different operating regimes of the quantum information engine to find optimal conditions for net work output and high engine performance.

Keywords: Quantum thermodynamics, quantum information engines, finite time, Quantum measurement, tradeoffs

Acknowledgements

I would like to extend my heartfelt thanks to my supervisor Henning Kirchberg for his guidance and patience, without whom this project would not have been possible. I would also like to thank Janine Splettstößer, and the rest of the Dynamics and Thermodynamics of Nanoscale Devices group. You made me feel welcome from day one and have made every day at the office both joyful and inspiring. I could not have asked for a better environment in which to write my master's thesis and to all of you, thank you.

Rasmus Hagman, Gothenburg, February 2025

List of Acronyms

BCH Baker-Campbell-Hausdorff. 18, 26

CNCA Chambadal-Novikov-Curzon-Ahlborn. xiv, 4, 10, 40–42

COP coefficient of performance. 28

GKSL Gorinski-Kossakowski-Sudarshan-Lindblad. 8

IE information engine. xiii, 13, 14, 28, 29, 31–34, 37, 45

QHO quantum harmonic oscillator. xiv, 2, 13–17, 19, 21, 23, 24, 28, 31, 37, 42, 45

QIE quantum information engine. 2, 3, 42, 45–47

RWA rotating wave approximation. 8

TLS two-level system. xiv, 2, 5, 10, 13–17, 19, 21–25, 28, 37, 38, 42, 45

Contents

List of Figures

List of Tables

1
Introduction

Thermodynamics has played a pivotal role in shaping our understanding of energy, heat, work, and the dynamics of macroscopic systems with its foundations dating back several centuries [1]. From the development of heat engines during the Industrial Revolution to the formulation of entropy and statistical mechanics, the field has continually evolved to address new scientific and technological challenges. Today, as nanoscale and quantum devices become more prevalent, how heat, work, and information flow at the quantum level are central questions in the field of quantum thermodynamics.

Thermodynamics at its foundation both facilitated and was propelled by the Industrial Revolution, particularly through the development of heat engines and the pursuit of a more rigorous understanding of extracting useful work from heat resources. The quest to understand the workings of heat engines eventually culminated in Sadi Carnot establishing the ideal so-called Carnot cycle, which provides a theoretical maximum bound on the efficiency of conversion of energy into useful work [2]. Importantly, the question arises as to which part of the energy is converted into useful work and which is dissipated as heat. In particular, how and in which direction energy is flowing when the engine is operating between two or more heat reservoirs. In this realm, Clausius was instrumental in defining entropy as

$$dS = \frac{Q}{T} \tag{1.1}$$

where dS represents the increase in entropy, Q denotes the heat, and T is the temperature of a heat reservoir [2]. With the formulation of the 2nd law of thermodynamics and the realisation that the total entropy never decreases, it was evident that heat can only flow spontaneously from a hotter to a colder reservoir, while useful work can be extracted. Boltzmann later provided a microscopic understanding of entropy with the equation

$$S = k_{\mathrm{B}} \ln \Omega \tag{1.2}$$

where k_{B} is the Boltzmann constant and Ω signifies the number of microstates for a given state of the system. Maxwell later explored the concept of entropy through his renowned thought experiment involving a "finite being" [3], later known as Maxwell's demon [4]. He imagined a closed box at thermodynamic equilibrium, divided into two sections by a partition. Maxwell proposed that if the demon could selectively open and close a gate in the partition to separate fast-moving particles from slow-moving ones, it would create a temperature gradient without performing any work. This would seem to violate the second law of thermodynamics, which states that entropy is always increasing. The apparent contradiction was later resolved by

incorporating the demon itself, and in particular its acquired information, into the system [5–8], something which is expanded in Section 2.2.2.

Today, nanoscale and quantum devices are becoming increasingly common, and the need to understand and manage the performance of transforming energy to useful work with these devices is becoming increasingly important [9]. Through feedback-controlled mechanisms, one can construct quantum information engines (QIEs) that takes advantage of information about the state of the engine to improve this energy conversion to useful work [5, 10–15], thus providing a potentially useful tool to make quantum devices more energy efficient. The information is acquired by measurements, which become a crucial step for the feedback process. An important step in the measurement process is the fact that the measurement result becomes an "objective" fact [16], i.e., the outcome and information acquired must be the same for different observers. An approach to modelling measurement behaviour is to consider a chain of meters that grows increasingly classical with each link in the chain [16, 17]. Nevertheless, in principle, there must be a cut at some point at which the quantum system has transitioned into a particular state with 100% probability, which is an indeterministic step in the quantum evolution. This point at which we introduce the system's transition into a particular state with 100% after measurement is the so-called Heisenberg cut. The Heisenberg cut is problematic since, in principle, quantum mechanics should be able to provide a description of all physical systems, yet we still do not have a clear definition of what measurement entails necessitating this discrete cut between quantum and classical [18]. Trying to cope with the measurement problem has spurred the development of several interpretations of quantum mechanics, the discussion of which is well beyond the scope of this thesis. In practice, this has not been a significant problem, as classical measurement devices have traditionally been large. With the development of nanodevices, however, the size of both systems and meters is decreasing and at some point the question of where and how the transition between quantum and classical occurs becomes important [18]. Classical measurements are typically modelled as instant, however, the claim in this thesis is that information transfer cannot be instantaneous but rather the meter and the system under measurement need to interact for some finite time during which information is transferred. In this thesis, we choose to model the system as a two-level system and the meter as a quantum harmonic oscillator, a sketch of the setup can be seen in Fig. 3.1, and a projective measurement is made of the quantum harmonic oscillator (QHO) rather than directly of the two-level system (TLS). When performing a measurement the state of the system is projected into the eigenstate corresponding to the measurement outcome [18], however, creating a pure state requires a diverging resource [19]. The diverging resource could be time, energy, or control complexity, meaning that if we desire our measurement to be finite in time and energy cost, it necessarily means a transition to a classical system with infinitely many degrees of freedom. Introducing a quantum meter does not fully resolve the issue of where the transition between quantum and classical occurs, as it raises the question of whether another quantum meter is needed to measure the first, leading to an infinite chain of measurement apparatuses. The measurement problem, determining when and how this transition takes place, remains an open question [18]. However, incorporating a quantum meter and shifting

the boundary between quantum and classical by even one step represents an effort to address this challenge. The quantum system-meter correlation is becoming an important resource as its correlation time sets a lower bound on the operation time of the feedback-controlled QIE.

1.1 Organization of the Thesis

As a guide for the reader, I choose to include a brief overview of how this thesis is organised. The work is purely theoretical; thus, the line between theory and method tends to blur. Nevertheless, I choose to separate theory and method to more clearly delineate between the work and analysis done during the project, and the theory necessary to understand the analysis. To that end, the structure of the thesis is as follows.

- Chapter 1 provides the historical context of the investigation, its motivations, and outlines the specific objectives of this study.
- Chapter 2 presents the theoretical framework necessary for understanding the subsequent analysis. This includes an overview of fundamental quantum mechanical principles in Section 2.1 and relevant thermodynamic concepts, such as the Szilard engine, in Section 2.2.
- Chapter 3 details the specific methodologies employed in this work, including the derivation of key quantities such as probability distributions and work measures. It also describes the QIE model, encompassing both unitary evolution and dissipative dynamics in the presence of a thermal bath.
- Chapter 4 presents the findings of this investigation, including cases of two different definitions of extracted work and including dissipative and non-dissipative evolutions.
- Chapter 5 discusses the implications of the results, provides concluding remarks, and offers an outlook with suggestions for future research.

1.2 Thesis Goals

The goal of this thesis is to understand the role of finite measurement time on the performance of a quantum information engine. Of particular interest is the role played by time and its impact on the performance of the QIE in terms of power production, under the assumption that the measurement time corresponds to the cycle time of the engine. As there are several free parameters in the model that will be considered, e.g. the temperatures that are involved, coupling strength, energy splittings, and time, a further goal is to also investigate what parameter regimes allow for positive work extraction, i.e. when the extracted work exceeds the energetic cost of measurement. An additional relevant performance quantifier is

efficiency, and a particularly relevant point of comparison is the Chambadal-Novikov-Curzon-Ahlborn (CNCA) efficiency, which is the maximum efficiency at maximum power.

2

Theory

This chapter presents the theory underlying the concepts used in this thesis to analyse quantum mechanical thermodynamic systems. Section 2.1 provides an introduction to density matrix formalism and the theory of open quantum systems, and Section 2.2 presents a brief introduction to thermodynamics and information theory.

2.1 Quantum Mechanics

While the quantum mechanical theory underpinning this thesis is extensive, it is assumed that the reader already has some familiarity with the subject. There are two main features to be introduced to the reader, the first being the density matrix formalism as an alternative to the usual wave functions and state vectors, this is presented in Section 2.1.1. The second is Markovian quantum master equations, detailing the evolution of a system under influence from a memoryless bath, and this is presented in Section 2.1.2.

2.1.1 Introduction to Density Matrices

In a closed quantum system, the state vector $|\psi\rangle$ describes the system and evolves in time according to the Schrödinger equation:

$$i\hbar\frac{\partial}{\partial t}|\psi(t)\rangle = \hat{H}(t)|\psi(t)\rangle\,, \tag{2.1}$$

where $\hat{H}(t)$ is the time-dependent Hamiltonian of the system. Rather than using wave functions or state vectors, another way to formulate quantum mechanics is through the density matrix formalism [20–22] which allows us to include a statistical description of the system. We could consider a collection of systems where each member is characterised by the state vector $|\varphi\rangle$, this is a pure state [21]. For a TLS, a pure state can be thought of as the state lying on the surface of the Bloch sphere [22, 23]. We could also consider a collection of systems in which the members are characterised by different state vectors $|\varphi_i\rangle$ with some relative population p_i, this is a mixed state [21]. Returning again to a TLS, a mixed state can be thought of as the states lying inside the Bloch sphere [22, 23]. In general, the density matrix corresponding to any quantum state can be written as a weighted sum over projectors on pure states [20–23],

$$\hat{\rho} = \sum_k p_k |\psi_k\rangle\langle\psi_k|\,. \tag{2.2}$$

The density matrix has a number of important properties:

$$\sum_k p_k = 1 \tag{2.3}$$

$$\mathrm{tr}\{\hat{\rho}\} = 1 \tag{2.4}$$

$$\langle\psi_k|\hat{\rho}|\psi_k\rangle \geq 0,\ \forall\ |\psi_k\rangle \tag{2.5}$$

$$\hat{\rho} = \hat{\rho}^\dagger \tag{2.6}$$

$$\mathrm{tr}\{\hat{\rho}^2\} \leq 1. \tag{2.7}$$

Equation (2.3) simply states that the population weights add up to one, Eqs. (2.4) to (2.6) state that the density matrix is a positive Hermitian operator of trace 1. In Eq. (2.7) the equality holds only for a pure state, and this property is sometimes called the purity of the state. Density matrices with $\mathrm{tr}\{\hat{\rho}^2\} < 1$ are mixed states and are statistical mixtures of pure states, and thus contain statistical uncertainties about the state. Perhaps the simplest way to highlight the difference between superposition and statistical uncertainties might be to consider the state $\hat{\rho}_1$ prepared in a superposition of $|0\rangle$ and $|1\rangle$, and to imagine that for $\hat{\rho}_2$ we have a uniformly random process generating either the state $|0\rangle$ or $|1\rangle$,

$$\hat{\rho}_1 = \frac{(|0\rangle + |1\rangle)(\langle 0| + \langle 1|)}{2}, \quad \hat{\rho}_2 = \frac{|0\rangle\langle 0| + |1\rangle\langle 1|}{2}. \tag{2.8}$$

In both cases a measurement in the basis $\{|0\rangle, |1\rangle\}$ will yield either $|0\rangle$ or $|1\rangle$ with equal probability. Changing basis to the computational basis

$$|+\rangle = \frac{|0\rangle + |1\rangle}{\sqrt{2}}, \quad |-\rangle = \frac{|0\rangle - |1\rangle}{\sqrt{2}} \tag{2.9}$$

yields

$$\hat{\rho}_1 = |+\rangle\langle +|, \quad \hat{\rho}_2 = \frac{|+\rangle\langle +| + |-\rangle\langle -|}{2} \tag{2.10}$$

meaning that $\hat{\rho}_2$ remains a mixture, while $\hat{\rho}_1$ is a pure state. Essentially, in Eq. (2.8) the uncertainty in the measurement outcome of $\hat{\rho}_1$ is fundamentally quantum in nature, while the uncertainty in measurement of $\hat{\rho}_2$ is due to ignorance of the preparation of the state.

One way to determine if a state is pure other than looking at the trace of the density matrix square is through the von Neumann entropy [22, 23],

$$S(\hat{\rho}) = -k_B\,\mathrm{tr}\{\hat{\rho}\ln\hat{\rho}\} \tag{2.11}$$

where if the density matrix is diagonalized we can write

$$S(\hat{\rho}) = -k_B \sum_k p_k \ln p_k \tag{2.12}$$

Calculating the von Neumann entropy for the two earlier cases yields

$$S(\hat{\rho}_1) = k_B \ln 1 = 0, \quad S(\hat{\rho}_2) = k_B \ln 2. \tag{2.13}$$

2.1.1.1 Equation of Motion for Density Matrices

For a system initially in a mixed state at time $t = 0$, the density matrix can be expressed as:

$$\hat{\rho}(0) = \sum_k w_k \left|\psi_k(0)\right\rangle \left\langle\psi_k(0)\right| . \tag{2.14}$$

As the system evolves, the state at a later time t can be determined using the time-evolution operator $\hat{U} = \mathcal{T} e^{-\frac{i}{\hbar}\int_0^t dt' H(t')}$ where $\mathcal{T}$ is the time-ordering operator, leading to:

$$\hat{\rho}(t) = \sum_k w_k \hat{U}(t) \left|\psi_k(0)\right\rangle \left\langle\psi_k(0)\right| \hat{U}^\dagger(t) = \hat{U}(t)\hat{\rho}(0)\hat{U}^\dagger(t). \tag{2.15}$$

Differentiating the above expression with respect to time yields the equation of motion for the density matrix:

$$\partial_t \hat{\rho}(t) = -\frac{i}{\hbar}[\hat{H}(t), \hat{\rho}(t)], \tag{2.16}$$

which is known as the von Neumann equation [21, 22].

It might not be the case that we are interested in how the entire system evolves, but rather that we are only interested in the dynamics of *part* of the system. For a system S that interacts with a thermal bath B, the total Hilbert space of the combined system is expressed as $\mathcal{H} = \mathcal{H}_\mathrm{S} \otimes \mathcal{H}_\mathrm{B}$. The Hamiltonian of the total system is given by:

$$\hat{H}(t) = \hat{H}_\mathrm{S} \otimes \hat{\mathbb{1}}_\mathrm{B} + \hat{\mathbb{1}}_\mathrm{S} \otimes \hat{H}_\mathrm{B} + \hat{V}_\mathrm{I}(t) = \hat{H}_\mathrm{S} + \hat{H}_\mathrm{B} + \hat{V}_\mathrm{I}(t), \tag{2.17}$$

where $\hat{\mathbb{1}}_S$ and $\hat{\mathbb{1}}_B$ are the identity operators on the Hilbert spaces of the system and bath, respectively, and $\hat{V}_\mathrm{I}(t)$ represents the interaction Hamiltonian between the system and the bath. In the final equality, the identity operators are omitted for simplicity. For subsequent discussions, identity operators will generally be implied, unless explicitly stated. As the degrees of freedom of the bath are not of interest and both the trace and partial derivative are linear operators we can trace out the bath by taking the partial trace over the bath and obtain [22]

$$\partial_t \hat{\rho}_\mathrm{S}(t) = -\frac{i}{\hbar} \mathrm{tr}_\mathrm{B} \left\{[\hat{H}(t), \hat{\rho}(t)]\right\} \tag{2.18}$$

where the partial trace of an operator $\hat{O} = \hat{A} \otimes \hat{B}$ is

$$\mathrm{tr}_\mathrm{A}\{\hat{O}\} = \sum_a \Big(\langle a| \otimes \mathbb{1}\Big)\hat{O}\Big(|a\rangle \otimes \mathbb{1}\Big) = \sum_a \langle a|\hat{O}|a\rangle . \tag{2.19}$$

2.1.2 Markovian Quantum Master Equations

Conceptually a master equation is an equation from which all other properties of a system can be derived [24]. Consequently, Eq. (2.18) can be perceived as a master equation, although solving it is often difficult. Nevertheless, with appropriate assumptions, one can deduce a Markovian master equation, widely recognised as

the Lindblad or Gorinski-Kossakowski-Sudarshan-Lindblad (GKSL) equation [22, 25–27]:

$$\partial_t \hat{\rho}(t) = -\frac{i}{\hbar}[\hat{H}, \hat{\rho}_{\mathrm{S}}] + \sum_k \gamma_k \mathcal{D}(\hat{L}_k)\hat{\rho}_{\mathrm{S}}, \tag{2.20}$$

where γ_k are the dissipation rates, $\hat{L}_k$ are the Lindblad jump operators, and $\mathcal{D}(\hat{L})$ is the dissipator, defined as

$$\mathcal{D}(\hat{L})\hat{\rho} = \hat{L}\hat{\rho}\hat{L}^\dagger - \frac{1}{2}\left\{\hat{L}^\dagger\hat{L}, \hat{\rho}\right\}, \tag{2.21}$$

with $\{\cdot,\cdot\}$ denoting the anticommutator. The jump operators $\hat{L}_k$ are typically determined from the microscopic model of the system dynamics, however, when describing the decay of a two-level system the jump operators will be the raising and lowering operators $\hat{a}^\dagger$, $\hat{a}$, sometimes denoted $\hat{\sigma}_+$, $\hat{\sigma}_-$ as in [22].

The Lindblad equation is widely used in quantum mechanics and quantum information to describe the dynamics of open quantum systems, capturing both the unitary evolution governed by the Hamiltonian $\hat{H}$ and dissipative processes represented by the dissipator. The Lindblad equation is typically derived from a microscopic description of the system, and the assumpions previously alluded to are:

- Weak coupling approximation: the coupling between the system and the bath is weak enough that the system only negligibly affects the bath [22, 24, 27]. This allows for a perturbative expansion in the coupling.
- Markov approximation: the bath correlation time is much shorter than the relaxation time of the system, making the bath memoryless [22, 24, 27]. This yields an equation that is local in time.
- Secular approximation: Also known as the rotating wave approximation (RWA), this neglects terms that oscillate rapidly in time [22, 24, 27]. This is common in quantum optics, but breaks down if the system energy gaps are small [27].

Detailed derivations from a microscopic background are plentiful; some examples can be found in [22, 24, 27].

2.2 Thermodynamics and Information

Thermodynamics typically deals with macroscopic systems with a large number of degrees of freedom. Classical thermodynamics is based on the four laws of thermodynamics [2, 28],

- Zeroth law: If A is in thermal equilibrium with B, and B is in thermal equilibrium with C, then A is in thermal equilibrium with C.
- First law: Energy is conserved, i.e. $\Delta U = Q + W$ where Q is the heat flowing into the system and W is the work done on the system.
- Second law: Entropy tends to increase, that is, $\Delta S \geq 0$.

- Third law: Entropy tends to a constant value as the temperature tends to zero, i.e. $\lim_{T\to 0} S(T) = S_0$.

Of particular importance for this work are the first and second laws.

One way of defining entropy is through the Gibbs entropy,

$$S_G = -k_\mathrm{B} \sum_s P(s) \ln P(s) \tag{2.22}$$

where the sum is over all the states of the system, and $P(s)$ is the probability of encountering that state. In this thesis, however, we are treating a quantum system. Thus we instead rely on the von Neumann entropy defined in Eq. (2.11). Using the definition of the density matrix, we note that $\hat{\rho}\,|\varphi_i\rangle = p_i\,|\varphi_i\rangle$ and $\ln\hat{\rho}\,|\varphi_i\rangle = \ln p_i\,|\varphi_i\rangle$, assuming the $\{|\varphi_i\rangle\}$ are orthogonal. Thus, the von Neumann entropy in ρ-eigenbasis is

$$S_\mathrm{vN} = -k_\mathrm{B} \sum_i \langle\varphi_i|\hat{\rho}\ln\hat{\rho}|\varphi_i\rangle = -k_\mathrm{B} \sum_i p_i \ln p_i \tag{2.23}$$

which is exactly the Gibbs entropy in Eq. (2.22). Interestingly, except for the factor k_B, it is also equal to the Shannon entropy [22, 23, 29, 30].

If the system of interest is a composite system, e.g. consisting of two or more separable components, we can define a conditional entropy. Conditional entropy quantifies the extent to which the entropy of one component is influenced by information about another component and we can define the conditional entropy of X given $Y = y$ as [23, 30]

$$S(X|y) = -k_\mathrm{B} \sum_{x\in X} P(x|y) \ln P(x|y) \tag{2.24}$$

where X, Y are two ensembles and x, y are the values of random variables distributed according to the ensembles X, Y. Using the conditional entropy we can define the mutual information I_m which quantifies the amount of information two systems contain about each other,

$$I_\mathrm{m}(X;Y) = S(X) - S(X|Y) = S(X) + S(Y) - S(X,Y) \tag{2.25}$$

where $S(X)$ is the marginal entropy of X, and $S(X,Y)$ is the joint entropy of X and Y. We can also note here that if the two distributions X and Y are uncorrelated, then $S(X,Y) = S(X) + S(Y)$ and as expected there is no mutual information between the two distributions. Thus when we have a system described by a density matrix $\rho(t)$ where $\rho(0) = \rho_1 \otimes \rho_2$ the mutual information between components one and two can be defined

$$I_\mathrm{m}(t) = S_\mathrm{vN}(0) - S_\mathrm{vN}(t). \tag{2.26}$$

2.2.1 Efficiency of Heat Engines

Heat engines are machines that convert heat into useful work. The general operating scheme is that the engine absorbs heat from a hot bath, which is then converted to work. However, in converting heat to work, the engine decreases the entropy of the hot bath. Consequently, only part of the heat can be converted into work. The

rest of the heat must be dumped as waste heat into the cold bath in order to either conserve or increase the overall entropy. The efficiency of a heat engine is limited by the Carnot efficiency [2]:

$$\eta_{\text{Carnot}} = 1 - \frac{T_{\text{c}}}{T_{\text{h}}} \tag{2.27}$$

where T_{c} and T_{h} are the cold and hot bath temperatures respectively. However, this efficiency can be reached only if the compression stage is adiabatic, meaning that the cycle time will approach infinity. The Carnot cycle thus yields an engine with maximum efficiency, but zero power [2, 31].

Another bound is the CNCA bound, which is an upper bound on efficiency at maximum power [31, 32]:

$$\eta_{\text{CNCA}} = 1 - \sqrt{\frac{T_{\text{c}}}{T_{\text{h}}}} \tag{2.28}$$

which, while not as fundamental as the Carnot efficiency, concerns finite-time operations and may therefore also serve as an intereseting point of comparison as this thesis will be dealing with finite cycle times.

2.2.2 The Szilard Engine and Feedback Controlled Processes

The Szilard engine is an early thought experiment that simplifies Maxwell's demon to a simple one-particle engine [5]. In [5], Szilard shows that work can indeed be extracted from a single heat bath using a feedback-controlled process [8, 10, 15, 33]. The principle of the Szilard engine is shown in Fig. 2.1, and Szilard's argument was the following. Assume that we have a box of volume V containing a single particle. At some time a partition is inserted, bisecting the box, rendering the position of the particle unknown. Assuming that the position of the particle is uniformly distributed, the probability of finding the particle in the left or right compartment is equal, $P_L = P_R = 1/2$, resulting in the entropy $k_{\text{B}}\left(-\frac{1}{2}\ln\frac{1}{2} - \frac{1}{2}\ln\frac{1}{2}\right) = k_{\text{B}}\ln 2$. Using the information about the particle's location; i.e. in the left or the right compartment, a load is attached to the correct side of the partition and the molecule is allowed to undergo isothermal adiabatic expansion, thus extracting work from a single heat bath. If we had no information about the location of the particle, the load would be attached at random, the result being that half of the time the load would be raised against gravity and half of the time the load would be lowered. If the information is not used, we would, on average, gain no work at all, so we see that the feedback process, that is, acting on the information gained through measurement, is what allows us to operate an engine that will produce useful work. Indeed, this will also be true for the engine discussed in Section 3.1, but even more pronounced as the population of the TLS is thermally distributed, meaning that the chance of failure is even greater, as the ground state will always be more likely than the excited state. A more detailed discussion will follow; this is merely to highlight why the feedback process is crucial. Noting that during isothermal adiabatic expansion the internal energy is constant, $dU = 0$, then with $TdS = dU - dW$ the work extracted, $-dW$, from the system is $k_{\text{B}}T\ln 2$.

If we assume that placing the partition necessitates no effort, it appears that we have managed to derive work from a system initially in thermal equilibrium without

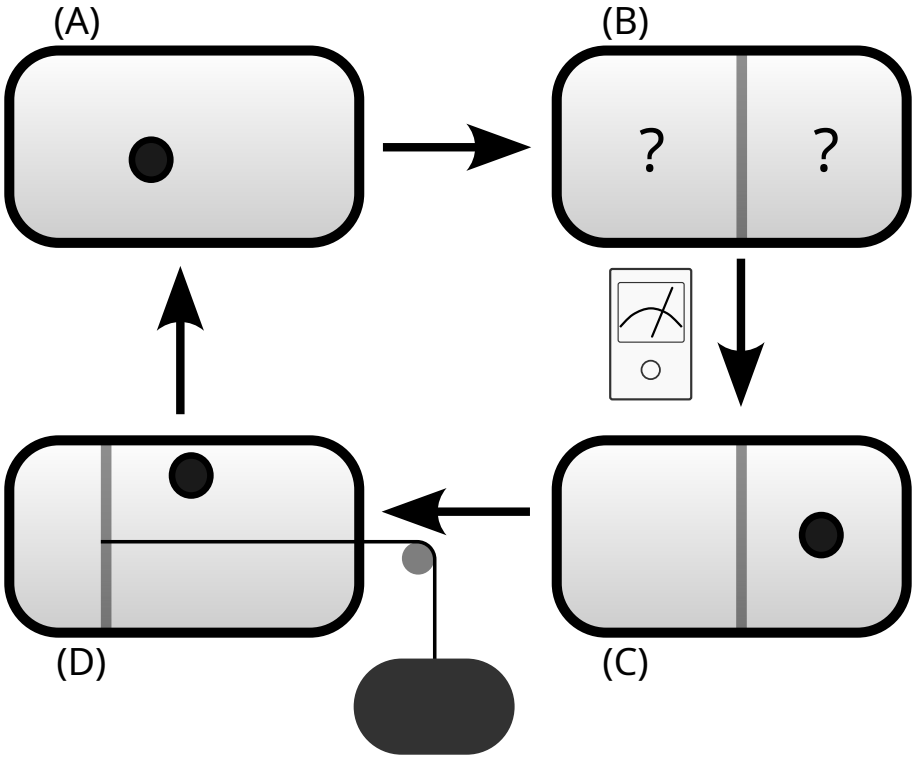

Figure 2.1: A schematic drawing of a Szilard engine [33]. (A) A particle in a closed box. (B) A partition is inserted, bisecting the box rendering the position of the particle unknown. (C) A measurement is made, indicating whether the particle is in the left or right compartment. (D) Attaching a load to the partition on the side of the particle and allowing the extraction of work via isothermal expansion.

having expended any work of our own. The apparent contradiction with the second law of thermodynamics is explained by considering that the measurement can be recorded in a single bit, such as assigning 1 to 'left' and 0 to 'right'. The minimal energy cost for erasing a single bit is given by $k_{\mathrm{B}}T\ln 2$ [7], which equals the work extracted. Thus, when erasure of the acquired information through measurement is taken into account, compliance with the second law is achieved. It is important to note that the memory's temperature does not necessarily need to match the temperature of the bath connected to the particle; rather, this represents an additional degree of freedom within the system.

3
Method

The primary aim is to extract work from a TLS by coupling it with a quantum meter, which in the context of this thesis is a QHO. The procedure for extracting work is dependent on the meter's state, conditional on the measurement outcome we either choose to extract work, or remain idle and wait for the next cycle. This is the feedback mechanism of the engine. Importantly, we assume that information cannot be transmitted instantaneously; instead, the system and the meter must be coupled for a finite duration to achieve correlation. This duration is referred to alternately as the correlation time, for apparent reasons, or the measurement time, given our assumption that the duration during which the meter is coupled to the system is the primary time scale within the system. Hence, we assume that the cycle time is equal to the measurement time, although in reality the measurement time only lower bounds the cycle time. In practice, the mechanism for extracting work is system dependent; one example could be a stimulated emission process.

This chapter begins with an introduction to the information engine (IE) model in Section 3.1, after which follows the derivation of key quantities such as probabilities and work. The analysis considers two cases:

- **Case 1: Non-dissipative evolution (Sec. 3.2)**
  In this scenario, the TLS and QHO are allowed to thermalise independently. Afterward, they are decoupled from their respective baths, ensuring that no dissipation occurs during the evolution.

- **Case 2: Dissipative evolution (Sec. 3.3)**
  Here, the coupling between the bath and the QHO is allowed to remain active during the evolution of TLS-QHO system thus allowing for dissipation via the meter.

3.1 The Information Engine Model

In this thesis, the IE model explored comprises a system and a meter, where the system, called the working medium, is a TLS, while the meter is represented by a QHO. Figure 3.1 illustrates this IE. In this configuration, the ground state energy of the TLS has been set to zero. The coupling of the TLS and the QHO results in their correlation, which leads to mutual information between them. The Hamiltonian of the system is

$$\hat{H}_{\mathrm{S}} = \Delta E \left|1\right\rangle \left\langle 1\right| \tag{3.1}$$

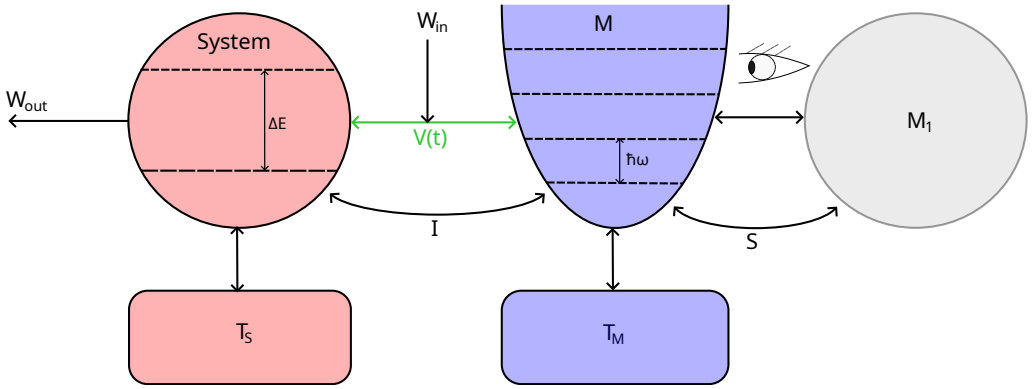

Figure 3.1: A general sketch of an information engine. A two-level system (TLS) (System) coupled to a meter (M) in the form of a quantum harmonic oscillator (QHO), each coupled to thermal baths of temperatures T_S and T_M respectively, with a coupling $V(t)$. The TLS and QHO exchange information I which is then used to extract work W_{out}. A second meter M1 performs a projective measurement of M resulting in entropy flow S between M1 and M.

where the excited state $|1\rangle$ has the energy ΔE and the ground state $|0\rangle$ has energy zero. The QHO Hamiltonian is

$$\hat{H}_{\mathrm{M}} = \frac{M\omega_0}{2}\hat{x}^2 + \frac{1}{2M}\hat{p}^2 \tag{3.2}$$

where M, ω_0 are the mass, frequency of the QHO and $\hat{x}$, $\hat{p}$ are the position, momentum operators. Hence, the total system Hamiltonian is

$$\hat{H} = \hat{H}_{\mathrm{S}} + \hat{H}_{\mathrm{M}} + \hat{V}_{\mathrm{I}}(t) = \Delta E\,|1\rangle\langle 1| + \frac{M\omega_0}{2}\hat{x}^2 + \frac{1}{2M}\hat{p}^2 + \hat{V}_{\mathrm{I}}(t) \tag{3.3}$$

where $\hat{V}_{\mathrm{I}}(t)$ is the coupling Hamiltonian defined as

$$\hat{V}_{\mathrm{I}}(t) = \begin{cases} g\,|1\rangle\langle 1| \otimes \hat{p}, & t \in (0, t_{\mathrm{m}}] \\ 0, & \text{otherwise.} \end{cases} \tag{3.4}$$

The measurement t_{m} is the time during which the coupling is switched on and g is the coupling strength. This means the QHO is only coupled to the excited state of the TLS where we later aim to extract its energy, and both TLS and QHO are initially coupled to thermal baths of finite temperatures T_{S} and t_{m}, respectively. The meter (the QHO) is then projectively measured in the Fock basis by a "Maxwell demon". The result of the measurement informs the "demon" whether the system (the TLS) has a higher probability of being in the excited state, prompting the "demon" to attempt work extraction, or if it is more probable that the system is in the ground state, in which case the "demon" decides to wait for the next cycle.

3.1.1 The Information Engine Cycle

The operation of an IE follows a cyclic process. This section offers an in-depth explanation of the cycle, which involves five primary stages: initialisation, the time

evolution stage where the system and meter establish a correlation, the measurement of the meter, the extraction of work from the system, and finally, restoring the entire system to its initial state to repeat the cycle. Following the structure laid out in [15] the different strokes of the engine are presented below.

1. Initial State

Initially, both TLS and QHO are assumed to be in thermal states at temperatures T_{S} and t_{m}, respectively. The initial state of the TLS is given by:

$$\begin{aligned}\hat{\rho}_S(0) &= \frac{1}{Z_0^S} e^{-\beta_S \hat{H}_{\mathrm{S}}} \\ &= \sum_i \frac{1}{Z_0^S} e^{-\beta_S E_i} \left|i\right\rangle \left\langle i\right| \\ &= \frac{1}{1+e^{-\beta_S \Delta E}} \left|0\right\rangle \left\langle 0\right| + \frac{e^{-\beta_S \Delta E}}{1+e^{-\beta_S \Delta E}} \left|1\right\rangle \left\langle 1\right| \\ &= a \left|0\right\rangle \left\langle 0\right| + b \left|1\right\rangle \left\langle 1\right|,\end{aligned} \tag{3.5}$$

where a and b are probabilities determined by the Gibbs distribution. Similarly, the initial state of the QHO is:

$$\hat{\rho}_M(0) = \frac{1}{Z_0} e^{-\beta_M \hat{H}_{\mathrm{M}}} = \sum_m \frac{1}{Z_0} e^{-\beta_M E_m} \left|m\right\rangle \left\langle m\right|, \tag{3.6}$$

where $\beta_i = \frac{1}{k_{\mathrm{B}} T_i}$, $i \in \{S, M\}$ is the inverse temperature, k_{B} is the Boltzmann constant, and $Z_0 = \mathrm{tr}\left\{e^{-\beta \hat{H}}\right\}$ is the partition function.

Thus, the total initial density matrix of the uncoupled system and meter is the tensor product of the individual density matrices:

$$\hat{\rho}_0 = \hat{\rho}_S(0) \otimes \hat{\rho}_M(0) = \left(a \left|0\right\rangle \left\langle 0\right| + b \left|1\right\rangle \left\langle 1\right|\right) \otimes \sum_m \frac{1}{Z_0} e^{-\beta E_m} \left|m\right\rangle \left\langle m\right|. \tag{3.7}$$

As the system and meter couple in the next stage there will be a shift in the energy splitting of the TLS, but the initial state is set at time $t = 0$, prrior to any effect by the coupling.

2. Time Evolution

During the time interval $(0,\, t_{\mathrm{m}})$, the system and the meter evolve under the influence of the Hamiltonian $\hat{H}$ (Eq. (3.3)) which includes the coupling Hamiltonian $V_I(t)$, resulting in an entangled state. The coupling is switched on instantly at time $t = 0$ and similarly switched off instantly at time $t = t_{\mathrm{m}}$. The density matrix at time t_{m} is given by:

$$\hat{\rho}(t_{\mathrm{m}}) = e^{-\frac{i t_{\mathrm{m}}}{\hbar} \hat{H}} \hat{\rho}_0 e^{\frac{i t_{\mathrm{m}}}{\hbar} \hat{H}}. \tag{3.8}$$

3. Measurement

At this stage, the system and meter are decoupled and a projective measurement is performed on the meter, collapsing the state of the meter to one of its energy

eigenstates $|n\rangle$. The joint probability of finding the TLS in state $|i\rangle$ and the QHO in state $|n\rangle$ at time t is:

$$P(i,n,t) = \langle i| \langle n|\hat{\rho}(t)|n\rangle |i\rangle . \tag{3.9}$$

The conditional probability of the TLS being in state $|i\rangle$ given that the QHO is in state $|n\rangle$ is:

$$P(i|n,t) = \frac{P(i,n,t)}{\sum_i P(i,n,t)} = \frac{P(i,n,t)}{P(n,t)}. \tag{3.10}$$

These probabilities are explicitly calculated in Section 3.2.1.

A key question to address is the amount of information gained at the end of this process, which can be divided into two components. The first component is mutual information, $I_{\mathrm{m}}(t)$, defined in Eq. (2.26), which is a measure of the amount of information shared between the system and the meter. Essentially, as the system and the meter co-evolve they will correlate and the mutual information is in a sense a measure of how much information about the TLS that is contained in the state of the QHO and vice versa. The second component relates to the observer, i.e. the "demon" or the feedback system, which performs the projective measurement. This is referred to as the *observer information*, $I_{\mathrm{obs}}(t)$ and is defined as:

$$\begin{aligned} I_{\mathrm{obs}}(t) = -k_{\mathrm{B}}\Big[& P(n \geq n', t) \ln\Big(P(n \geq n', t)\Big) \\ & + \Big(1 - P(n \geq n', t)\Big) \ln\Big(1 - P(n \geq n', t)\Big)\Big], \end{aligned} \tag{3.11}$$

where n' is the activation threshold for the feedback mechanism, i.e., when the observer initiates an attempt to extract work, the significance of which will be discussed in Section 3.2.2.2. Specifically:

- The states $\{|n_i\rangle\}_{i=n'}^{\infty}$ will activate the feedback mechanism.
- The states $\{|n_i\rangle\}_{i=0}^{n'-1}$ will not activate the feedback mechanism.

The observer information quantifies the uncertainty faced by the "demon" about whether or not the measurement outcome has exceeded n' where n' is the threshold at which we try to extract work in one of the schemes that will be presented later. Essentially this represents the "demons" uncertainty about whether or not it should try to extract work or not. Hence, when making a measurement on the meter the outcome of the measurement gives the "demon" information about the system due to the correlation between system and meter as a result of their coupling. The total amount of information gained is $I(t_{\mathrm{m}}) = I_{\mathrm{m}}(t_{\mathrm{m}}) + I_{\mathrm{obs}}(t_{\mathrm{m}})$.

4. Work Extraction

We assume that if the TLS is in the excited state, we can extract the full energy of the excited state, ignoring the potential energetic costs of the extraction process itself. We use two measures for the average extracted work per cycle, excess work $W_{\mathrm{ext}}^{\mathrm{exc}}$ and ergotropy $W_{\mathrm{ext}}^{\mathrm{erg}}$, which are discussed in more detail in Sections 3.2.2.2 and 3.2.2.3.

5. Resetting

The cycle is closed by letting both the TLS and the QHO rethermalize in contact with their baths at temperatures T_{S} and t_{m}, respectively, while remaining decoupled from each other. The demon's memory must also be reset. However, its temperature, T_{D}, is not necessarily equal to the system or the meter temperature; instead, it represents an additional degree of freedom. Choosing to set $T_{\mathrm{D}} = 0$ as in [34] means that the second law is upheld due to the erasure of information and the energy balance is unaffected as the erasure work is $k_{\mathrm{B}}T_{\mathrm{D}} \ln 2 = 0$. Setting $T_{\mathrm{D}} \neq 0$ would negatively impact the engine's overall performance, yet since there is no obvious or natural choice for T_{D} and its value likely depends on the specific physical implementation, we choose to set it to zero. It should be noted that this will impact the estimate of efficiency as a non-zero T_{D} will increase the amount of done on the system while the work extracted from the TLS will be unchanged.

3.2 Non-Dissipative Evolution

The initial phase of the analysis involves examining the non-dissipative progression of the complete system as governed by the Hamiltonian given in Eq. (3.3), which entails maintaining unitary evolution by excluding coupling with a bath. The starting condition of the entire system is represented by Eq. (3.7), with the time evolution of the density matrix expressed by Eq. (3.8). A first step is to diagonalize the Hamiltonian and to that end we rewrite the Hamiltonian as

$$\hat{H} = \left(\Delta E - \frac{Mg^2}{2}\right) |1\rangle \langle 1| + \frac{1}{2M} \left(\hat{p} + Mg\, |1\rangle \langle 1|\right)^2 + \frac{M\omega^2}{2}\hat{x}^2. \tag{3.12}$$

The energy of the TLS experiences a displacement known as a Stokes shift, and there is also a shift in the momentum operator. To eliminate the shift in the momentum operator, we employ the shift operator

$$\hat{D} = e^{iMg|1\rangle\langle 1|\otimes\hat{x}/\hbar} \tag{3.13}$$

and observe that both shift operators and time evolution operators are unitary, $\hat{D}\hat{D}^\dagger = \hat{\mathbf{1}}$ and $\hat{U}(t)\hat{U}^\dagger(t) = \hat{\mathbf{1}}$, to yield the density matrix

$$\begin{aligned}
\hat{\rho}(t) &= \hat{D}^\dagger \hat{D} e^{-it\hat{H}/\hbar} \hat{D}^\dagger \hat{D} \hat{\rho}(0) \hat{D}^\dagger \hat{D} e^{it\hat{H}/\hbar} \hat{D}^\dagger \hat{D} \\
&= \hat{D}^\dagger e^{-it\hat{H}_0/\hbar} \hat{D} \hat{\rho}(0) \hat{D}^\dagger e^{it\hat{H}_0/\hbar} \hat{D} \\
&= e^{-it\hat{H}_0/\hbar} \hat{D}^\dagger(t) \hat{D} \hat{\rho}(0) \hat{D}^\dagger \hat{D}(t) e^{it\hat{H}_0/\hbar}
\end{aligned} \tag{3.14}$$

where

$$\hat{H}_0 = \Delta\tilde{E}\, |1\rangle \langle 1| + \frac{1}{2M}\hat{p}^2 + \frac{M\omega^2}{2}\hat{x}^2 \tag{3.15}$$

$$\hat{D}(t) = e^{iMg|1\rangle\langle 1|\otimes\hat{x}(t)/\hbar} \tag{3.16}$$

$$\hat{x}(t) = \hat{x}(0)\cos(\omega t) + \frac{\sin(\omega t)}{M\omega}\hat{p}(0) \tag{3.17}$$

with $\Delta\tilde{E} = (\Delta E - \frac{Mg^2}{2})$

Next, we use the Baker-Campbell-Hausdorff (BCH) formula $e^{\hat{X}}e^{\hat{Y}} = e^{\hat{Z}}$ with $\hat{Z} = \hat{X} + \hat{Y} + \frac{1}{2}\left[\hat{X}, \hat{Y}\right] + ...$ to combine the shift operators. Letting $\hat{x}(0) = \hat{x}_0$ and $\hat{p}(0) = \hat{p}_0$ we focus on the factor $\hat{D}^\dagger(t)\hat{D}$ and evaluate the commutator:

$$\begin{aligned}
&\frac{M^2g^2}{\hbar^2}\left|1\right\rangle\left\langle 1\right| \otimes \left[-i\left(\cos(\omega t)\hat{x}_0 + \frac{\sin(\omega t)}{M\omega}\hat{p}_0\right), i\hat{x}_0\right] \\
&= \frac{M^2g^2}{\hbar^2}\frac{\sin(\omega t)}{m\omega}\left|1\right\rangle\left\langle 1\right| \otimes [\hat{p}_0, \hat{x}_0] \\
&= -i\frac{Mg^2\sin(\omega t)}{\hbar\omega}\left|1\right\rangle\left\langle 1\right|.
\end{aligned} \tag{3.18}$$

It also becomes clear that the higher-order commutators that appear in the BCH formula, that is, the commutators on the form $[\hat{X}, [\hat{X}, \hat{Y}]]$, are zero. Therefore, the expression for $\hat{Z}$ is:

$$\hat{Z} = i\frac{Mg}{\hbar}\left|1\right\rangle\left\langle 1\right|\left(-\hat{x}(t) + \hat{x}(0) - \frac{g\sin(\omega t)}{2\omega}\right) \tag{3.19}$$

we observe that the term $\frac{g\sin(\omega t)}{2\omega}$ is a scalar and, therefore, it commutes with all other components in $\hat{\rho}(t)$ and can easily be factored out by writing $\hat{D}^\dagger(t)\hat{D} = e^{Z_2}e^{Z_1}$ where $Z_2 = -\frac{iMg}{\hbar}\frac{g\sin(\omega t)}{2\omega}$. When evaluating $\hat{D}^\dagger\hat{D}(t)$ a corresponding e^{-Z_2} appears meaning that the $e^{\pm Z_2}$ terms will cancel. Consequently, this term is omitted in the analysis, resulting in

$$\hat{Z} = -i\frac{Mg}{\hbar}\left|1\right\rangle\left\langle 1\right|\left(\Big(\cos(\omega t) - 1\Big)\hat{x}(0) + \frac{\sin(\omega t)}{M\omega}\hat{p}(0)\right) \tag{3.20}$$

$$\hat{D}^\dagger(t)\hat{D} = e^{\hat{Z}}. \tag{3.21}$$

Using the relations [20, 21]

$$\hat{x} = \sqrt{\frac{\hbar}{2M\omega_0}}(\hat{a}^\dagger + \hat{a}) \tag{3.22}$$

$$\hat{p} = i\sqrt{\frac{\hbar M\omega_0}{2}}(\hat{a}^\dagger - \hat{a}) \tag{3.23}$$

and switching to the annihilation and creation operators the combined shift operator can be written

$$\hat{D}(\alpha) = e^{\alpha(t)\hat{a}^\dagger - \alpha^*(t)\hat{a}} \tag{3.24}$$

$$\alpha(t) = g\sqrt{\frac{M}{2\hbar\omega_0}}\left(\sin(\omega_0 t) - i\Big(\cos(\omega t) - 1\Big)\right). \tag{3.25}$$

In conclusion the density matrix at time t due to the time-evolution in presence of coupling is

$$\hat{\rho}(t) = e^{-it\hat{H}_0/\hbar}\hat{D}(\alpha)\hat{\rho}_0\hat{D}^\dagger(\alpha)e^{it\hat{H}_0/\hbar} \tag{3.26}$$

where it's worth noting that the entire time dependence is contained in the α parameter defined in Eq. (3.25).

3.2.1 Joint and Conditional Probabilities

Calculating the joint and conditional probabilities introduced in Eqs.(3.9, 3.10) there are two probabilities to calculate, the probability of the TLS being in the ground state, $|0\rangle$, given some measurement outcome n and the probability of the TLS being in the excited state, $|1\rangle$, given some measurement outcome n.

3.2.1.1 Joint Probability in the Absence of Interaction

Referring to Eq. (3.9) the joint probability of the TLS being in state $|0\rangle$ and the QHO being in state $|n\rangle$ at time t will be

$$P(0,n,t) = \langle 0| \langle n|\hat{\rho}(t)|n\rangle |0\rangle . \tag{3.27}$$

The meter only couples to the $|1\rangle$ state, hence there is no contribution from the interaction term and the joint probability is

$$\begin{aligned} P(0,n,t) &= \langle 0| \langle n| \hat{\rho}(t) |n\rangle |0\rangle \\ &= \langle 0| \langle n| e^{-it\hat{H}_0/\hbar}(a|0\rangle\langle 0| + b|1\rangle\langle 1|) \otimes \sum_m P_m |m\rangle\langle m| e^{it\hat{H}_0/\hbar} |n\rangle |0\rangle \\ &= a\sum_m P_m \langle n|m\rangle\langle m|n\rangle = aP_n \\ &= a\frac{1}{Z_0} e^{-\beta_M \hbar\omega_0(n+1/2)}. \end{aligned} \tag{3.28}$$

3.2.1.2 Joint Probability in the Presence of Interaction

When the system is in the excited state, it couples to the meter and the evaluation is less straightforward. We make use of the result from Eq. (3.26) and express the joint probability as

$$\begin{aligned} P(1,n,t) &= \langle 1| \langle n| e^{-it\hat{H}_0/\hbar} \hat{D}(\alpha)\hat{\rho}_0\hat{D}^\dagger(\alpha) e^{it\hat{H}_0/\hbar} |n\rangle |1\rangle \\ &= b\sum_m P_m \langle n| \hat{D}(\alpha) |m\rangle \langle m| \hat{D}^\dagger(\alpha) |n\rangle \\ &= b\sum_m P_m \left|\langle n| \hat{D}(\alpha) |m\rangle\right|^2 . \end{aligned} \tag{3.29}$$

An identity from [35]

$$\langle m|\hat{D}(\alpha)|n\rangle = \left(\frac{n!}{m!}\right)^{1/2} \alpha^{m-n} e^{-|\alpha|^2/2} L_n^{(m-n)}(|\alpha|^2) \tag{3.30}$$

along with an identity for the generalised Laguerre polynomials from [36]

$$L_n^{(-k)}(x) = (-x)^k \frac{(n-k)!}{n!} L_{n-k}^{(k)}(x) \tag{3.31}$$

are useful to yield

$$P(1,n,t) = \begin{cases} b\sum_m P_m \left| \left(\frac{m!}{n!}\right)^{1/2} \alpha^{n-m} e^{-|\alpha|^2/2} L_m^{(n-m)}(|\alpha|^2) \right|^2, & n \geq m \\ b\sum_m P_m \left| \left(\frac{n!}{m!}\right)^{1/2} (-\alpha^*)^{m-n} e^{-|\alpha|^2/2} L_n^{(m-n)}(|\alpha|^2) \right|^2, & m > n \end{cases} \tag{3.32}$$

where α is defined in Eq. (3.25) and $L_p^{(k)}$ are the generalized Laguerre polynomials. The motivation to reformulate the displacement operator as presented in Eq. (3.24) is primarily based on the identity discussed in [35]. It should be noted that, from a mathematical perspective, there is no need to distinguish between two separate cases in Eq. (3.32), as the initial case remains valid even when $n < m$. The distinction is made here because some widely-used implementations of the generalised Laguerre polynomials in programming languages, notably the function provided by SciPy [37], cannot handle inputs with $n - m < 0$, necessitating a reformulation with the second case. Conditional probabilities are derived from the definition in Eq. (3.10), applying the outcomes from Eqs. (3.28) and (3.32).

3.2.2 Assessing Work Extraction and Costs

When calculating the net extracted work from the system, we need to account for both the cost of measurement W_{meas} and the work extracted from the system W_{ext}. The cost of the measurement, or the measurement work, is presented in Section 3.2.2.1. Two different measures have been used for the work extracted from the system, the excess work discussed in Section 3.2.2.2, and the ergotropy discussed in Section 3.2.2.3.

3.2.2.1 Cost of Measurement

The work associated with switching the coupling between system and meter on and off we call the measurement work, W_{meas}, and define it as

$$W_{\text{meas}}(t_{\text{m}}) = \text{tr}\left(\hat{\rho}_0 \hat{V}\right) - \text{tr}\left(\hat{\rho}(t_{\text{m}})\hat{V}\right) \tag{3.33}$$

where the first term is the work required to couple and the second term is the work to decouple the system and meter. Examining each of the terms on their own, starting with the coupling work yields

$$\begin{aligned}
&\text{tr}\left(\hat{\rho}(t=0)\hat{V}\right) \\
&= \sum_n \sum_i \langle n| \langle i| \left(a |0\rangle \langle 0| + b |1\rangle \langle 1|\right) \otimes \sum_m e^{-\beta E_m} |m\rangle \langle m| \left(g |1\rangle \langle 1| \otimes \hat{p}\right) |i\rangle |n\rangle \\
&= bg \sum_m \sum_n \frac{e^{-\beta E_m}}{Z_0} \langle n|m\rangle \langle m|\hat{p}|n\rangle = bg \sum_m \sum_n \frac{e^{-\beta E_m}}{Z_0} \langle m|\hat{p}|n\rangle \langle n|m\rangle \\
&= bg \sum_m \frac{e^{-\beta E_m}}{Z_0} \langle m|\hat{p}|m\rangle = 0
\end{aligned} \tag{3.34}$$

meaning that turning on the coupling requires no work in this model. Examining the second term is more involved,

$$\text{tr}\left(\hat{\rho}(t)\hat{V}\right) = bg \sum_n \sum_m \left\langle n \left| \hat{p} e^{-it\hat{H}/\hbar} \right| m \right\rangle \left\langle m \left| e^{it\hat{H}/\hbar} \right| n \right\rangle \tag{3.35}$$

and again the unitarity of the displacement operator is utilized and inserted strategically

$$\text{tr}\left(\hat{\rho}(t)\hat{V}\right) = bg \sum_m e^{-\beta E_m} \langle m|\hat{D}^\dagger(t)\hat{D}\hat{p}\hat{D}^\dagger\hat{D}(t)|m\rangle \,. \tag{3.36}$$

Using commutators and the commutator relation $[f(\hat{x}), \hat{p}] = i\hbar\frac{df(x)}{dx}$ the density operator can be migrated from the centre to the left of the operator product by

$$[f(\hat{x}), \hat{p}] = f(\hat{x})\hat{p} - \hat{p}f(\hat{x}) \Leftrightarrow f(x)\hat{p} = i\hbar\frac{df(x)}{dx}\hat{\mathbb{1}} + \hat{p}f(x) \tag{3.37}$$

where $f(x)$ will be the shift operators $\hat{D}$. To save space, I show only the more involved case of the time-dependent shift operator, however, the procedure is the exact same for the time-independent shift operators. We note that $\hat{D}^\dagger(t) = e^{-iMg\hat{x}(t)/\hbar} = \exp\left(\frac{-iMg}{\hbar}\left(\hat{x}\cos(\omega_0 t) + \hat{p}\frac{\sin(\omega_0 t)}{M\omega_0}\right)\right)$ and $\hat{p}$ commutes with itself, so only the $\hat{x}$ part contributes. Thus

$$\hat{D}^\dagger(t)\hat{p} = i\hbar\frac{d}{dx}e^{\hat{x}(t)}\hat{\mathbb{1}} + \hat{p}\hat{D}^\dagger(t) = (Mg\cos(\omega_0 t) + \hat{p})\hat{D}^\dagger(t) \tag{3.38}$$

and applying this idea with both $\hat{D}^\dagger$ and $\hat{D}^\dagger(t)$ to Eq. 3.36 results in

$$\mathrm{tr}\left(\hat{\rho}(t)\hat{V}\right) = -bg^2M\Big(1 - \cos(\omega_0 t)\Big) \tag{3.39}$$

making the total W_{meas}

$$W_{\mathrm{meas}} = \mathrm{tr}\left(\hat{\rho}(0)\hat{V}\right) - \mathrm{tr}\left(\hat{\rho}(t)\hat{V}\right) = bg^2M\Big(1 - \cos(\omega_0 t)\Big) \tag{3.40}$$

where M is the mass of the QHO, g is the coupling strength between system and meter, and b is the initial population in the excited state of the TLS defined in Eq. (3.5).

3.2.2.2 Excess Energy as a Measure of Extracted Work

A method to define extracted work is by what is termed excess work. Typically, incident photons on resonance with a TLS induce one of two processes: absorption when the TLS is in the ground state, or stimulated emission when in the excited state. The excess work concept examines the work extractable from a system after correlation with a meter, compared to the work extractable at time $t = 0$ when in a thermal state. This idealised stimulated emission process effectively disregards absorption, instead focussing on the increased likelihood of achieving stimulated emission given some additional information about the state of the system obtained through measurement compared to the case without this additional information. In particular, systems that start in thermal equilibrium invariably exhibit a net energy loss when absorption is considered. Therefore, while considering excess energy as a work metric might not be an ideal engine operation scheme, it does assess how measurement enhances engine efficacy.

Accordingly, the excess work is defined as [15]:

$$W_{\mathrm{ext}}^{\mathrm{exc}}(t) = \sum_{n=n'}^{N} P(n,t)\left[P(1|n,t) - P(1|n,t=0)\right]\Delta E \tag{3.41}$$

where $P(n,t) = \sum_i P(i,n,t)$ and n' is the energy eigenstate threshold where the demon chooses to extract work, i.e. when measuring a population in states $n \geq n'$

the demon attempts to extract work. The requirement for an activation threshold can be understood as follows. Without an activation threshold, merely summing over all possible states of the meter results in making no deliberate choice, which means that we attempt to extract work at each cycle without utilising the gained information. Conversely, if we limit the attempts to extract work, such as exclusively trying to induce stimulated emission when the meter is in a state $|n'\rangle$, $n' > 0$, we effectively use the information to guide our actions. As for how to choose n' we can refer to Fig. 4.11 which shows the conditional probabilities of being in the ground state (blue) and being in the excited state (orange) as a function of the measurement outcome n. The solid lines are the initial state populations and the dotted lines are the populations after some time t_m. When using excess work n' is chosen such that $P(1|n, t_\mathrm{m}) > P(1|n, t = 0)$, i.e., at the first orange dot lying above the solid orange line. Or in other words, when the measurement outcome is in regions II-IV an attempt to extract work is made.

At $t = 0$ $P(1|n, t = 0) = b$ and the extracted work becomes

$$\begin{aligned} W_\mathrm{ext}^\mathrm{exc} &\equiv \Delta E \sum_{n=n'}^{\infty} P(n,t)\left(P(1|n,t) - b\right) \\ &= \Delta E \sum_{n=n'}^{\infty} \left[\Big(P(0,n,t) + P(1,n,t)\Big)\left(\frac{P(0,n,t)}{P(0,n,t)+P(1,n,t)} - b)\right)\right] \\ &= \Delta E \sum_{n=n'}^{\infty} \left[P(1,n,t) - b\Big(P(1,n,t) + P(0,n,t)\Big)\right] \\ &= \Delta E \sum_{n=n'}^{\infty} \left[aP(1,n,t) - bP(0,n,t)\right] \end{aligned} \tag{3.42}$$

where the relation $a + b = 1$, and Bayes' rule was used.

3.2.2.3 Ergotropy as a Measure of Extracted Work

A concept to introduce here is ergotropy, the maximum amount of work that can be extracted from a quantum system under unitary transformations [38, 39]:

$$W_\mathrm{ext}^\mathrm{erg} = \mathrm{tr}\left\{\hat{\rho}_\mathrm{S}(t_\mathrm{m})\hat{H}_\mathrm{S}\right\} - \sum_n P(n,t_\mathrm{m}) \min_n \mathrm{tr}\left\{\hat{U}_n \hat{\rho}_{\mathrm{S|n}} \hat{U}_n^\dagger\right\} \tag{3.43}$$

meaning that to extract work we apply a unitary transformation $\hat{U}_n$, which will depend on the measurement outcome n. The first term on the right-hand side is the energy of the system after measurement but prior to any work extraction. The second term gives the energy of the system after extraction, averaged over all possible measurement outcomes. To maximise the extracted work, we choose the unitary transformation that minimises the energy of the final state of the system.

Each measurement outcome corresponds to a different unitary transformation; however, in each case, the unitary transformation that maximises the extracted work will be population inversion for a TLS. Thus, averaging over all possible measurement outcomes, the ergotropy will be

$$W_\mathrm{ext}^\mathrm{erg}(t_\mathrm{m}) = \Delta E \sum_{n=0}^{\infty} P(n,t)\left[P(1|n,t_\mathrm{m}) - P(0|n,t_\mathrm{m})\right]\Theta(P(1|n,t_\mathrm{m}) - P(0|n,t_\mathrm{m})) \tag{3.44}$$

where the Heaviside function Θ accounts for the transition from an active state, where $P(1|n,t_\mathrm{m}) > P(0|n,t_\mathrm{m})$, to a passive state, where $P(0|n,t_\mathrm{m}) > P(1|n,t_\mathrm{m})$. Once again employing Bayes' rule yields

$$W_\mathrm{ext}^\mathrm{erg}(t_\mathrm{m}) = \Delta E \sum_{n=0}^{\infty} \left[P(1,n,t_\mathrm{m}) - P(0,n,t_\mathrm{m})\right] \Theta(P(1|n,t_\mathrm{m}) - P(0|n,t_\mathrm{m})) \tag{3.45}$$

where the key distinction in comparison to Eq. (3.41) lies in comparing $P(1,n,t_\mathrm{m})$ to $P(0,n,t_\mathrm{m})$ rather than $P(1,n,t=0)$.

3.3 Effects of a Thermal Bath on System Evolution

Up to this point, the system has been considered closed during the evolution, meaning the evolution has been unitary. This implies that there has been no external influence or leakage into or out of the TLS or QHO. However, it has initially been assumed that there are thermal baths, as indicated by TLS and QHO achieving thermal equilibrium through contact with their respective thermal baths. In this section, the QHO is connected to a thermal bath with temperature T_M throughout the time evolution of the system, altering the system from a closed quantum system to an open one. This connection introduces dissipative effects, leading to a non-unitary evolution of the system and the meter. Although the evolution of the complete system, including the bath, stays unitary, the reduced dynamics of the system and meter alone is non-unitary.

The first step in this analysis is to modify the Hamiltonian by incorporating the bath and the bath-meter coupling into the Hamiltonian presented in Eq. (3.3):

$$\hat{H} = \Delta E \left|1\right\rangle \left\langle 1\right| + \frac{1}{2M}\hat{p}^2 + \frac{M\omega^2}{2}\hat{x}^2 + \hat{V}_I + \sum_k \hbar\omega_k \hat{b}_k^\dagger \hat{b}_k + \sum_k g_k \hat{x}_k \otimes \hat{x}, \tag{3.46}$$

where the bath Hamiltonian and the bath-meter coupling Hamiltonian are given by:

$$\hat{H}_B = \sum_k \hbar\omega_k \hat{b}_k^\dagger \hat{b}_k, \tag{3.47}$$

$$\hat{H}_{BM} = \sum_k g_k \hat{x}_k \otimes \hat{x}, \tag{3.48}$$

with $\hat{b}_k, \hat{b}_k^\dagger$ as the bosonic annihilation and creation operators of the bath and g_k as the bath-meter coupling strengths.

The coupling between the bath and the meter by the $\hat{x}$ operator is chosen because $\hat{x}$ commutes with the shift operator defined in Eq. (3.13). This allows for the same transformation of the total Hamiltonian as in Sec. 3.2, yielding:

$$\hat{H} = \hat{D}^\dagger \hat{H}_0 \hat{D} + \hat{H}_B + \hat{H}_{BM}. \tag{3.49}$$

Examining the bath-meter interaction Hamiltonian, we have:

$$\begin{aligned}\hat{H}_{BM} &= \hat{x} \otimes \sum_k g_k \hat{x}_k = (\hat{a}^\dagger + \hat{a}) \otimes \sum_k \tilde{g}_k \left(\hat{b}_k^\dagger + \hat{b}_k\right) \\ &= \sum_k \tilde{g}_k \left(\hat{a}^\dagger \hat{b}_k^\dagger + \hat{a}^\dagger \hat{b}_k + \hat{a}\hat{b}_k^\dagger + \hat{a}\hat{b}_k\right) \\ &\approx \sum_k \tilde{g}_k \left(\hat{a}^\dagger \hat{b}_k + \hat{a}\hat{b}_k^\dagger\right),\end{aligned} \tag{3.50}$$

where the prefactors have been absorbed into $\tilde{g}_k$, and non-energy-conserving terms have been neglected in the final step. This yields an interaction Hamiltonian of the same form as the standard damped oscillator, as discussed in [22, 24].

Although deriving a Lindblad equation for the density operator using the full Hamiltonian in Eq. (3.49) is theoretically possible, the coupling between QHO and TLS complicates the picture, making it difficult to achieve an analytic expression for the density operator and consequently also for the probabilities. Instead, it is assumed that the coupling is weak enough so that the dissipation can be treated as occurring entirely through the position operator of the meter. The master equation is then employed:

$$\begin{aligned}\partial_t \hat{x} = i\omega_0[\hat{a}^\dagger \hat{a}, \hat{x}] + \gamma_0(\bar{n}+1)\left(\hat{a}\hat{x}\hat{a}^\dagger - \frac{1}{2}\left(\hat{a}^\dagger\hat{a}\hat{x} + \hat{x}\hat{a}^\dagger\hat{a}\right)\right) \\ +\gamma_0\bar{n}\left(\hat{a}^\dagger\hat{x}\hat{a} - \frac{1}{2}\left(\hat{a}\hat{a}^\dagger\hat{x} + \hat{x}\hat{a}\hat{a}^\dagger\right)\right)\end{aligned} \tag{3.51}$$

where the $\hat{x}$ operator can be rewritten as $\sqrt{\frac{\hbar}{2M\omega_0}}(\hat{a}^\dagger + \hat{a})$ and γ_0 is the dissipation rate. All the operators are linear and so the equation can be split in two parts,

$$\sqrt{\frac{\hbar}{2M\omega}}\partial_t \hat{a}^\dagger = \sqrt{\frac{\hbar}{2M\omega}}\left(i\omega[\hat{a}^\dagger\hat{a}, \hat{a}^\dagger] + \gamma_0(\bar{n}+1)\mathcal{D}[\hat{a}^\dagger]\hat{a}^\dagger + \gamma_0\bar{n}\mathcal{D}[\hat{a}]\hat{a}^\dagger\right) \tag{3.52}$$

$$\sqrt{\frac{\hbar}{2M\omega}}\partial_t \hat{a} = \sqrt{\frac{\hbar}{2M\omega}}\left(i\omega[\hat{a}^\dagger\hat{a}, \hat{a}] + \gamma_0(\bar{n}+1)\mathcal{D}[\hat{a^\dagger}]\hat{a} + \gamma_0\bar{n}\mathcal{D}[\hat{a}]\hat{a}\right). \tag{3.53}$$

Solving each of the equations separately yields

$$\hat{a}^\dagger(t) = e^{(i\omega - \gamma_0/2)t}\hat{a}^\dagger(0) \tag{3.54}$$

$$\hat{a}(t) = e^{-(i\omega + \gamma_0/2)t}\hat{a}(0) \tag{3.55}$$

resulting in

$$\hat{x}(t) = e^{-\gamma_0 t/2}\left(\cos(\omega t)\hat{x} - \frac{\sin(\omega t)}{M\omega}\hat{p}\right). \tag{3.56}$$

Comparing Eq. (3.56) with the undamped, time-dependent position operator (Eq. (3.17)) the effect of the coupling to the bath is an exponential damping over time.

The procedure from this point follows a similar approach to that described in Section 3.2. The density matrix is given by:

$$\hat{\rho}(t) = e^{-i\hat{H}t/\hbar}\hat{\rho}_0 e^{i\hat{H}t/\hbar} = e^{-i\hat{H}t/\hbar}\hat{D}^\dagger(t)\hat{D}\hat{\rho}_0\hat{D}^\dagger\hat{D}(t)e^{i\hat{H}t/\hbar}, \tag{3.57}$$

where, as before, $\hat{H}$ is defined in Eq. (3.15). However, in this case, the time dependence of the shift operators is governed by Eq. (3.56), rather than Eq. (3.17).

By applying the same procedure for combining shift operators, the density matrix takes a form analogous to Eq. (3.26). In this formulation, the entire time dependence, and consequently the damping effect, is contained in the parameter α, which is now modified to:

$$\alpha(t) = g\sqrt{\frac{M}{2\hbar\omega_0}}\left(e^{-\gamma_0 t/2}\sin(\omega_0 t) - i\left(e^{-\gamma_0 t/2}\cos(\omega_0 t) - 1\right)\right). \tag{3.58}$$

It should be noted that by setting the dissipation rate to zero, $\gamma_0 = 0$, Eq. (3.58) simplifies to Eq. (3.25). Although this result is expected, it serves as a useful consistency check.

It is pertinent to briefly compare the dissipative case with the unitary case discussed in Section 3.2. In both cases, measurement work, defined as the work required to couple and decouple the system and the meter, remains unaffected by dissipation. Similarly, the extracted work along any individual trajectory continues to be 0 or ΔE. The primary effect of dissipation lies in the loss of information, which modifies the probabilities derived in Section 3.2.1. Consequently, there is no need to revisit the expressions for the measurement work W_{meas}, or the extracted work, W_{ext}. However, as information is continuously leaking from the meter to the bath, the probabilities must be recalculated to account for this leakage of information.

3.3.1 Probabilities in the Dissipative Case

The calculation of joint probabilities in the dissipative case closely follows the method outlined in Section 3.2.1, with the difference being the use of the dissipative evolution of the displacement operator.

For the ground state, the situation mirrors the unitary case discussed in Section 3.2.1.1. In this scenario, there is no coupling between the system and the meter, leaving the meter unaffected. Since the meter is already in a thermal equilibrium state with the bath at temperature T_{M}, there is no dissipation. As a result, the joint probability $P(0, n, t)$ remains identical to the expression derived in Section 3.2.1.1, following Eq. (3.28).

For the TLS in the excited state, the coupling between the system and the meter is active, as in the unitary case. The procedure described in Section 3.2.1.2 can still be applied, with the key modification that the time evolution of the operator $\hat{x}$ is now governed by Eq. (3.56). Despite this adjustment, the approach of rewriting the shift operators as the quantum optics displacement operator remains valid. Thus, the joint probabilities are calculated once again using Eq. (3.32), with the parameter $\alpha(t)$ now defined by Eq. (3.58).

3.4 The Zeno Limit

A noteworthy special case is the behaviour of the system in the so-called Zeno limit. This limit corresponds to the regime of very frequent measurements, or in the

idealised scenario, continuous measurement, which slows or even completely stops the evolution of the quantum system under observation [40, 41]. In the context of this thesis, frequent measurements are effectively represented by measurements with very short correlation times. The question is whether a criterion can be established for the positive extraction of net work, that is, when $W_{\text{ext}} - W_{\text{meas}} > 0$. For the general case, it is difficult to obtain an informative closed-form expression for this inequality. However, the Zeno limit allows for a simplified analysis.

In the Zeno limit, short correlation times imply timescales that are small compared to all relevant physical processes. In this analysis, three primary timescales are considered. The first is the period of the quantum harmonic oscillator (QHO), which requires $\omega_0 t \ll 1$. The second time scale refers to the rate of information exchange between the system and the meter, requiring $gt \ll 1$, where g is the coupling strength between the system and the meter. The third timescale is the dissipation rate from the meter to the bath, to ensure minimal information leakage, the condition $\gamma_0 t \ll 1$ must also be satisfied, however, since the coupling to the bath is already assumed to be weak, this is readily fulfilled.

3.4.1 The Zeno Condition of Excess Work

Starting from the unitary case, we consider the inequality $W_{\text{ext}}^{\text{exc}}(t_m) > W_{\text{meas}}(t_m)$, where $W_{\text{ext}}^{\text{exc}}(t_m)$ and $W_{\text{meas}}(t_m)$ are defined by Eqs. (3.41) and (3.33), respectively:

$$ab\Delta E \left[\sum_{n=n'}^{\infty} \sum_{m} e^{-\beta_M \hbar\omega_0 m} \langle n|e^{-i\frac{Mg}{\hbar}\hat{x}(t)} e^{i\frac{Mg}{\hbar}\hat{x}}|m\rangle \langle m|e^{-i\frac{Mg}{\hbar}\hat{x}} e^{i\frac{Mg}{\hbar}\hat{x}(t)}|n\rangle - \frac{e^{-\beta_M \hbar\omega_0 n'}}{1-e^{-\beta_M\hbar\omega_0}} \right] > bMg^2\Big(1-\cos(\omega_0 t)\Big) \tag{3.59}$$

where it is pertinent to point out that n' is fixed "from outside", i.e., it is chosen by the observer. Here, the shift operators are expressed as defined in Eqs. (3.16) and (3.13). Now we Taylor expand around $\omega_0 t = 0$, utilize the canonical commutation relation $[\hat{x}, \hat{p}] = i\hbar$ [20, 21], and apply the BCH formula yielding

$$\sum_{n=n'}^{\infty} \sum_{m} \langle n|e^{-i\frac{gt}{\hbar}\hat{p}}|m\rangle \langle m|e^{i\frac{gt}{\hbar}\hat{p}}|n\rangle - \frac{e^{-\beta_M\hbar\omega_0 n'}}{1-e^{-\beta_M\hbar\omega_0}} > \frac{Mg^2\omega_0^2 t^2}{2a\Delta E(1-e^{-\beta_M\hbar\omega_0})}. \tag{3.60}$$

Using the second condition, $gt \ll 1$, we expand to second order and repeatedly use the fact that $\langle n|m\rangle = \delta_{nm}$, where $|n\rangle$ and $|m\rangle$ are Fock states and δ_{nm} is the Kronecker delta. This simplifies to:

$$\sum_{n=n'}^{\infty} \sum_{m} e^{-\beta_M\hbar\omega_0 m} \left[\langle n|\hat{p}|m\rangle \langle m|\hat{p}|n\rangle - \frac{\delta_{nm}}{2}\Big(\langle n|\hat{p}^2|m\rangle + \langle m|\hat{p}^2|n\rangle \Big) \right] > \frac{M\hbar^2\omega_0^2}{2a\Delta E(1-e^{-\beta_M\hbar\omega_0})}. \tag{3.61}$$

Expressing the momentum operator $\hat{p}$ in terms of the annihilation and creation operators, $\hat{a}$ and $\hat{a}^\dagger$, and simplifying further, we find:

$$\sum_{n=n'}^{\infty} \sum_{m} e^{-\beta_M\hbar\omega_0 m}(-1)\Big[\langle n|\hat{a}^\dagger - \hat{a}|m\rangle \langle m|\hat{a}^\dagger - \hat{a}|n\rangle \Big] + \sum_{n=n'}^{\infty} \langle n|\hat{a}^{\dagger 2} + \hat{a}^2 - \hat{a}\hat{a}^\dagger - \hat{a}^\dagger\hat{a}|n\rangle\,. \tag{3.62}$$

Using the relations $\hat{a}\,|n\rangle = \sqrt{n}\,|n-1\rangle$ and $\hat{a}^\dagger\,|n\rangle = \sqrt{n+1}\,|n+1\rangle$, the Kronecker delta collapses the sum, leading to:

$$\sum_{n=n'}^{\infty}\left[ne^{-\beta_M\hbar\omega_0(n-1)} + (n+1)e^{-\beta_M\hbar\omega_0(n+1)} - (2n-1)e^{-\beta_M\hbar\omega_0 n}\right] > \frac{\hbar\omega_0}{a\Delta E(1-e^{-\beta_M\hbar\omega_0})}. \tag{3.63}$$

Applying the differentiation trick:

$$e^x\sum_n ne^{-xn} = e^x\sum_n -\partial_x e^{-xn}, \tag{3.64}$$

and simplifying, we eventually arrive at the condition for the Zeno limit:

$$n'\left(1-e^{\beta_M\hbar\omega_0}\right)^2 e^{-\beta_M\hbar\omega_0(n'+1)} > \frac{\hbar\omega_0}{a\Delta E}. \tag{3.65}$$

This condition is independent of both the time and the coupling strength, which seems odd. Interestingly, the condition derived is independent of both time and the coupling strength, which is somewhat unexpected. While I am currently unable to provide a definitive explanation for this behaviour, it is worth noting that one might reasonably anticipate the coupling strength to influence the condition, given its explicit role in the measurement work, so the absence of the coupling strength in the final condition is noteworthy. To determine the parameter regime in which positive net work extraction is possible, we may replace the inequality with an equality; solving the resulting equation then provides the boundary of this regime. All numerical simulations conducted indicate that the extracted work is maximised when $n' = 1$. Although a general proof of this behaviour is lacking, this consistent outcome motivates the focus on the case $n' = 1$. Under this assumption, the condition simplifies to

$$4e^{-\beta_M\mu\Delta E}\sinh^2\left[\frac{-\beta_M\mu\Delta E}{2}\right] - \frac{\mu}{a} = 0 \tag{3.66}$$

with $\mu = \frac{\hbar\omega_0}{\Delta E}$.

3.4.2 The Zeno Condition of Ergotropy

If instead the extracted work is taken to be the ergotropy, the inequality to investigate is $W_{\text{ext}}^{\text{erg}}(t_m) > W_{\text{meas}}(t_m)$ with $W_{\text{ext}}^{\text{erg}}(t_m)$ defined in Eq. (3.44). The steps are generally the same as those taken Section 3.4.1, and the inequality is

$$\Delta E\sum_{n=n'}^{\infty}\left[\sum_m\left(\frac{b}{Z_0}e^{-\beta_M\hbar\omega_0(m+1/2)}\,\langle n|\hat{D}^\dagger(t)\hat{D}|m\rangle\,\langle m|\hat{D}^\dagger\hat{D}(t)|n\rangle\right) - \frac{a}{Z_0}e^{-\beta_M\hbar\omega_0(n+1/2)}\right] > bMg^2\Big(1-\cos(\omega_0 t)\Big) \tag{3.67}$$

with $\hat{D}$ defined in Eq. (3.13). In this case n' is given by the definition of ergotropy and depends on time, and specifically $n' = \min\{n : P(1|n,t_m) > P(0|n,t_m)\}$. The end result is the following condition:

$$4n'(t)\sinh^2\left(\frac{\beta_M\hbar\omega_0}{2}\right) > \frac{\hbar\omega_0}{\Delta E}e^{\beta_M\hbar\omega_0 n'(t)} + \frac{\hbar(a-b)}{g^2M\omega_0 t^2 b}. \tag{3.68}$$

Although the condition is superficially similar to the result in Eq. (3.65), there are differences. The two main differences are that the condition using ergotropy now depends explicitly on both time, t, and what we call the effective coupling strength, $g_{\text{eff}} = g\sqrt{M}$.

3.5 Performance Quantities

In considering the efficiency of the setup, it is useful to keep in mind the different operating regimes in order to find a reasonable definition of efficiency. Figure 3.2 shows a schematic explanation of the different regimes. As the engine always extracts work from the TLS, the work that is extracted from the engine must correspond to the heat flowing out of the bath coupled to the TLS. Equally, the assumption is made that whatever work we put into coupling and decoupling system and meter will be dumped into the bath coupled to the meter (QHO). Hence, we define four regions:

- If $T_{\text{M}} < T_{\text{S}}$ and $W_{\text{net}} = W_{\text{ext}} - W_{\text{meas}} > 0$, then we extract work which is heat flowing out of the hot bath. This is a heat engine (HE).
- If $T_{\text{M}} < T_{\text{S}}$ and $W_{\text{net}} < 0$, then we perform work to remove heat from the hotter bath. This is a heat valve (HV).
- If $T_{\text{M}} > 0$ and $W_{\text{net}} < 0$, then we perform work to cool the colder bath. This is a refrigerator (RF).
- If $T_{\text{M}} > T_{\text{S}}$ and $W_{\text{net}} > 0$, then we extract work while also cooling the colder bath. This is not something we could expect to reach in a classical setup, so this is what we call the information engine regime (IE).

It is important to note that while we choose to name the fourth case the IE regime, the entire system is an IE and every other case also makes use of information to drive the engine. Defining efficiency, or coefficient of performance (COP), is essentially defining a benefit/cost ratio, and in the case of a heat engine, the benefit is the work carried out by the engine, whereas the cost is the heat that flows from the system bath. In the case of a heat valve or refrigerator, the benefit is the heat flowing out of the system bath and the cost is the work put in to drive the cycle. Thus we define the efficiencies or COPs as follows:

$$\eta_{\text{HE}} \equiv \frac{W}{|Q_{\text{S}}|} = 1 - \frac{W_{\text{meas}}}{W_{\text{ext}}} \tag{3.69}$$

where the final equality has used the definition $Q_{\text{S}} = -W_{\text{ext}}$, $Q_{\text{M}} = W_{\text{meas}}$. Basically, the work we extract must be the heat flowing out of the system, and for the measurement work the assumption is that the work put in to couple and decouple system and meter will eventually flow into the meter bath as heat. In both the refrigeration and heat valve regimes the COP can be defined as

$$COP \equiv \left|\frac{Q_{\text{S}}}{W}\right|. \tag{3.70}$$

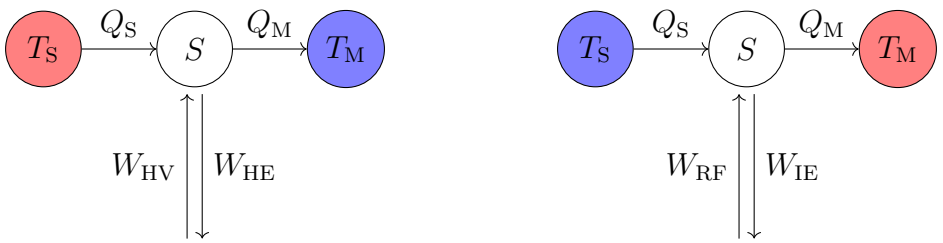

Figure 3.2: Schematic explanation of the different operating regimes of the IE. On the left, the case $T_S > T_M$, and on the right the case when $T_S < T_M$. Note in particular the case of W_{IE} on the right, which is specifically the IE regime. Following the discussion in Section 3.5 four different regimes are defined. The heat engine (HE), heat valve (HV), refrigerator (RF), and the information engine (IE).

In the IE regime the useful action is extraction of work and cooling of the system bath, at the cost of the measurement work, yielding

$$\eta_{IE} \equiv \frac{W + |Q_S|}{Q_M}. \tag{3.71}$$

When considering excess work, it is important to recognize that, while this quantity can serve as a useful indicator of how information may enhance engine performance, it does not necessarily provide an accurate measure of the engine's actual efficiency. This limitation arises from the assumption that the underlying process is purely one of stimulated emission, neglecting the possibility of absorption events. As a result, the definition of excess work omits a potentially significant source of energy loss.

Consequently, defining an efficiency in analogy with that used in ergotropy-based analyses can be misleading. This issue will become evident in Chapter 4, where the calculated efficiency appears to exceed the Carnot limit. It is important to emphasize that this apparent violation is not indicative of a fundamental breach of the Carnot bound, but rather reflects the incomplete accounting of losses in the current model.

3.6 Simulations

The data set used to investigate and analyse the system's behaviour was generated via simulations. Within these simulations, quantities such as measurement work and extracted work were computed using the equations detailed in Chapters 2 and 3. To define several crucial variables, the approach adopted was to parameterize them by correlating each with the system temperature, thereby enabling the use of several dimensionless parameters. Parameterisation involves expressing the different variables in terms of system temperature T_S along with a dimensionless parameter:

- $T_M = xT_S$
- $\Delta E = C_S k_B T_S$

- $\hbar\omega_0 = C_\mathrm{M} k_\mathrm{B} T_\mathrm{S}$
- $g\sqrt{m} = P\sqrt{k_\mathrm{B} T_\mathrm{S}}$
- $t_\mathrm{m} = \frac{2\pi}{\omega_0}\tau$
- $\gamma_0 = R\omega_0$.

Here x, C_S, C_M, P, τ, R are the dimensionless parameters and varying x for example is analogous to varying the temperature of the meter; varying τ would vary the measurement time t_m, etc. What this does is that it completely eliminates T_S as a parameter and lets us vary only the dimensionless parameters, making the simulation easier and more numerically robust.

The simulations were carried out using the Python programming language [42], in conjunction with the Numpy [43] and SciPy [37] libraries for numerical computations. Figures were made using Matplotlib [44] and Seaborn [45].

4

Results and Discussion

This chapter presents the results obtained from the simulations and analyses performed during the project. In the figures, the time is given in the dimensionless quantity ωt where, t is the correlation time, or measurement time, and $\frac{2\pi}{\omega}$ is the period of the QHO. Essentially, the time is given in terms of the period of the harmonic oscillator. This choice of units allows for a more intuitive comparison across different timescales.

4.1 Short Measurement Times: Zeno-limit

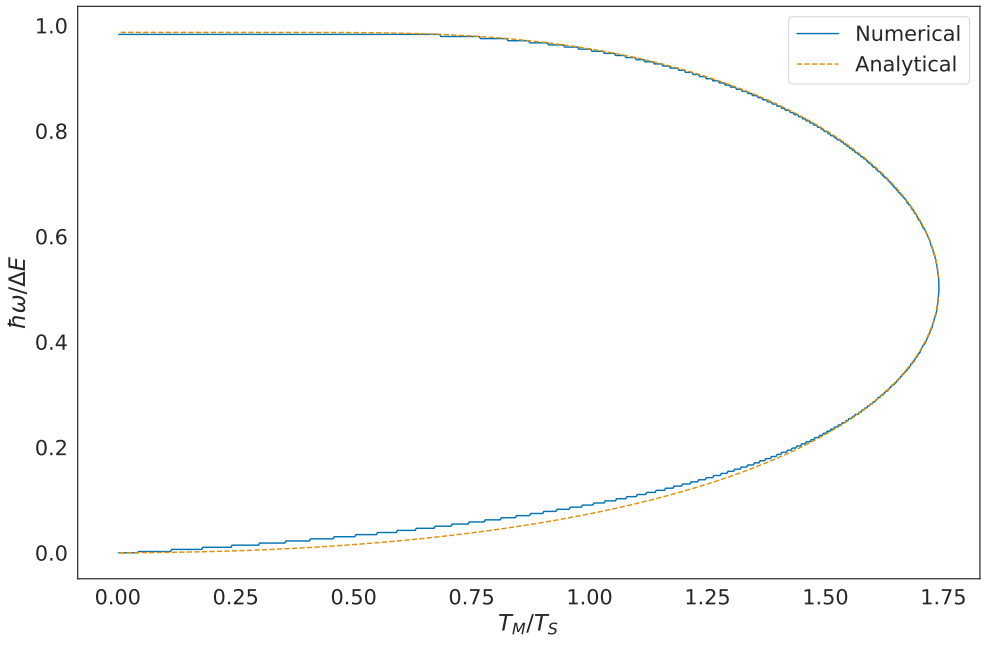

Figure 4.1: Comparison between the dissipative simulations of the IE in the Zeno limit relying on W_{ext}^{exc}, and the numerical solution to the Zeno limit phase boundary for $n' = 1$ given in Eq. (3.66).

In Section 3.4, an expression was derived for the boundary that separates net positive and net negative work in the Zeno limit. Specifically, the activation threshold for $n' = 1$ is given by Eq. (3.66). To validate this analytical result, a comparison between the numerically solved analytical expression and the results of direct numerical simulations is presented in Fig. 4.1.

What Fig. 4.1 shows is the analytical result in the dashed orange line and the numerical results in the solid blue line. The area inside the curve is where the extraction of the work is net positive and the area outside the curve is net negative. For a clearer description of the different regions, see Fig. 4.2 where this case is the top left plot. The agreement is good in the upper half of the curve; in the lower half of the curve there is a discrepancy between the numerical and analytical results. The cause of this discrepancy is unknown, but I offer a few possibilities that could have been explored with more time to explain this disagreement. Essentially, I see three main possibilities: an error in the simulation, an error in the derivation of the condition that yields Eq. (3.66), or an error in solving Eq. (3.66). The discussion should be preceded with an explanation of how the figure was generated. The numerical data come from running a simulation with the same model as all the other data used to generate the figures in this thesis. It was a simple case of stepping through many different values of $\frac{\hbar\omega}{\Delta E}$ and many different values of $\frac{T_\mathrm{M}}{T_\mathrm{S}}$, calculating the net work, $W_\mathrm{ext}^\mathrm{erg} - W_\mathrm{meas}$, and finding where the sign of the output work changes. The analytical curve is produced by numerically solving Eq. (3.66). However, due to the shape of the curve, this solution was divided into two parts, the upper half and the lower half of the analytic curve were found separately and then joined to create the hyperbola shown in Fig. 4.1. If the simulation is incorrect, it seems, at least to me, unlikely that the top halves of the numerical and analytical results should agree almost perfectly. It is possible that the specific combination of $\frac{\hbar\omega}{\Delta E}$ and $\frac{T_\mathrm{M}}{T_\mathrm{S}}$ produced some slight numerical instability, but I cannot see where this would appear or why. The second option is that there is an error in the derivation of the condition in the first place. However, by the same argument that it would seem highly unlikely that the upper halves should agree almost perfectly, this does not seem like a good explanation. The third option is that there is an error in the numerical solution of Eq. (3.66). This might be possible, numerically solving equations can be sensitive to the inputs given to the solver. However, I am not proficient enough regarding numerical methods to say with any certainty if this is cause of the discrepancy here. In short, the cause of the discrepancy remains unknown.

Two conditions were found for positive net work extraction in the short-time limit, or the Zeno limit, one for each measure of extracted work. These conditions, Eqs. (3.65) and (3.68), are superficially similar but differ in two key aspects, namely the effective coupling strength, $g_\mathrm{eff}^2 = g^2 M$ and the time squared, t^2, both appear in the condition using ergotropy as the measure of extracted work and do not when using excess work as the measure. However, in both cases, as shown later in, e.g. Figs. 4.4 and 4.5, the power output drastically decreases in the Zeno limit. Although it may be possible to extract power using continuous measurement, it is not clear to me that treating it as an engine cycle is the most natural description. If the measurement is truly continuous, the question arises of when the system should be allowed to return to its initial state, as it must in a cyclical process.

4.2 Different Operating Regimes

Figure 4.2 illustrates the phase diagram for the unitary evolution of the IE. For com-

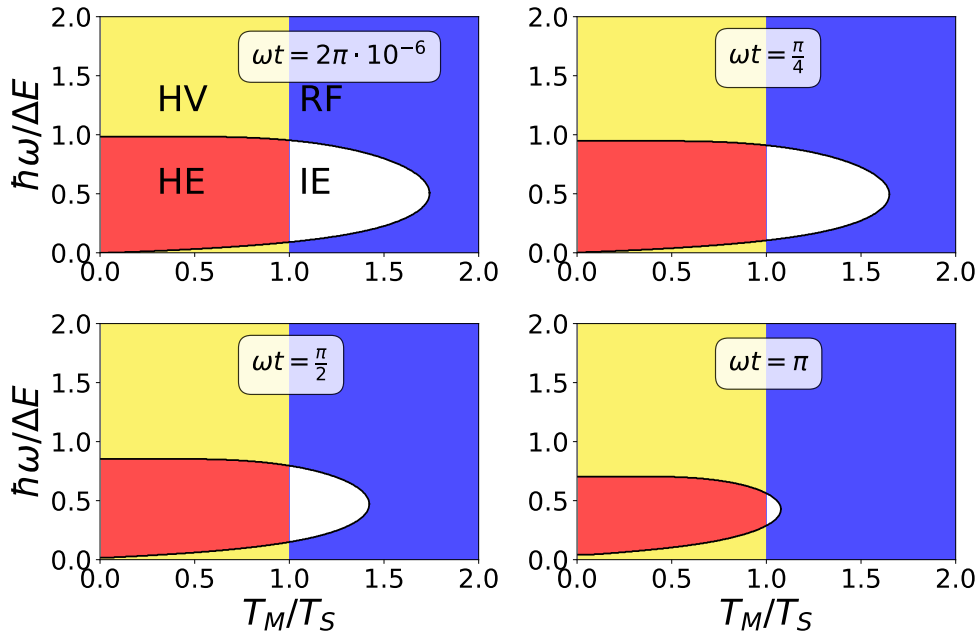

Figure 4.2: Phase diagram of the unitary, i.e. $\gamma = 0$, IE at different times relying on $W_{\text{ext}}^{\text{exc}}$. The red area corresponds to a classical heat engine, the yellow to a heat pump, the blue to a refrigerator, and the white to what we call the "true" IE regime. The black line denotes the boundary between net positive and negative work production. For a schematic explanation of the phases refer to Fig. 3.2

parison, the corresponding phase diagram for the dissipative case, with a dissipation rate of $\gamma = \omega \cdot 10^{-1}$, is shown in Fig. 4.3. The value $\gamma = \omega \cdot 10^{-1}$ at least reasonable, it has been used in other analyses of harmonic oscillators and qubit-oscillator systems [46, 47]. The two figures are similar, but there is a clear difference in the $\omega t = \pi$ case, when

4.2.1 Discussion of Working Regimes for Excess Work

It should be noted that the phase diagrams presented in this subsection use only excess work as a quantifier of extracted work. As for why the corresponding diagrams using ergotropy are not shown, the reason is that I have not found any set of parameters that allow positive net work extraction in the case when $T_{\text{M}} > T_{\text{S}}$, making a phase diagram less interesting.

Figs. 4.2 and 4.3 show four distinct regions. The HV, RF, and HE regions are not very surprising. The engine being able to move heat around as in the HV and RF regions or

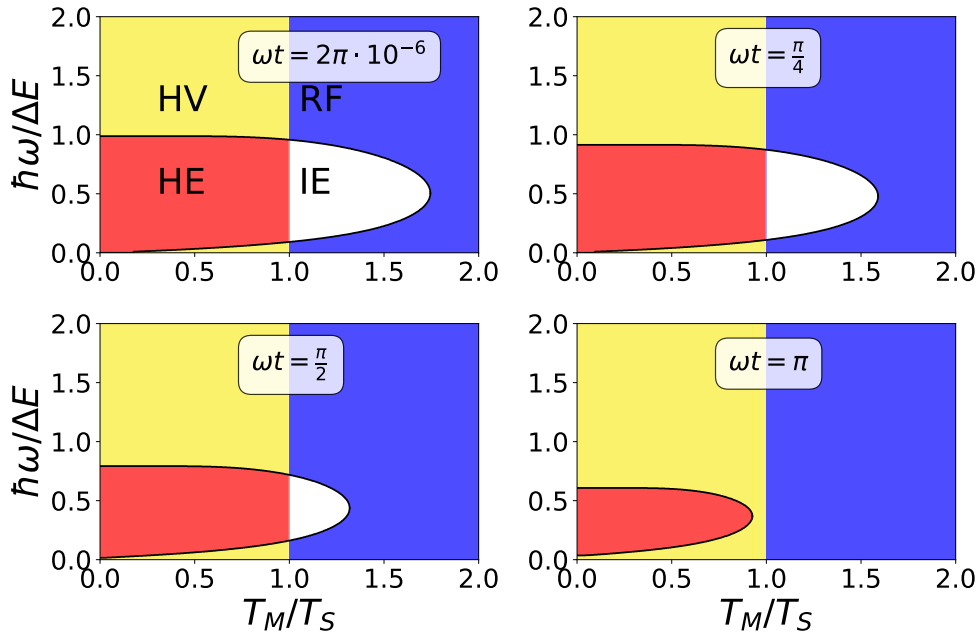

Figure 4.3: Phase diagram of the IE with a dissipation rate $\gamma = \omega/10$, using W_{ext} The red area corresponds to a classical heat engine, the yellow to a heat pump, the blue to a refrigerator, and the white to what we call the "true" IE regime. The black line denotes the boundary between net positive and net negative work production. For a schematic explanation of the phases refer to Fig. 3.2

4.3 Influence of Temperature, Energy Splitting, and Coupling Strength on Power Output

In this section, we investigate the performance of the engine by examining its power output when varying the quantities $\frac{T_{\text{M}}}{T_{\text{S}}}$, $\frac{\hbar\omega}{\Delta E}$, $\frac{g^2_{\text{eff}}}{\Delta E}$. We begin by analysing how $\frac{T_{\text{M}}}{T_{\text{S}}}$ and $\frac{\hbar\omega}{\Delta E}$ affect both the net power,

$$\Pi(t_{\text{m}}) = \frac{W_{\text{ext}} - W_{\text{meas}}}{t_{\text{m}}}, \tag{4.1}$$

and the ergotropy defined in Eq. (3.44). Heatmaps are presented to show the behaviour of these quantities and how they change at different times. Subsequently, the same analysis is carried out showing how $\frac{T_{\text{M}}}{T_{\text{S}}}$ and $\frac{g^2_{\text{eff}}}{\Delta E}$ affect power and ergotropy.

4.3.1 Dependence on Temperature and Energy Spacing

Figures 4.4 and 4.5 present heatmaps of net power generation, where power is defined in Eq. (4.1). Red indicates positive power output (engine) and blue indicates negative output (heat valve or refrigerator). The x-axis represents the relative temperature $\frac{T_{\text{M}}}{T_{\text{S}}}$, while the y-axis represents the relative energy spacing $\frac{\hbar\omega}{\Delta E}$. Each figure includes four subplots at various normalised times: a very short time to mimic continuous measurement, and times at $\frac{1}{8}$, $\frac{1}{4}$, and $\frac{1}{2}$ of the harmonic oscillator period.

After one full period, the meter is back in its original position and no longer contains any information about the system. We can look at the joint probabilities to see this, where $P(0, n, t_\mathrm{m})$ is time independent (Eq. (3.28)), and for $P(1, n, t_\mathrm{m})$ (Eq. (3.32)) the time dependence is given by the α parameter (Eq. (3.25)) which is zero in one full period, just as in time $t = 0$. Thus, the power will only be lower at longer times than one period of the harmonic oscillator.

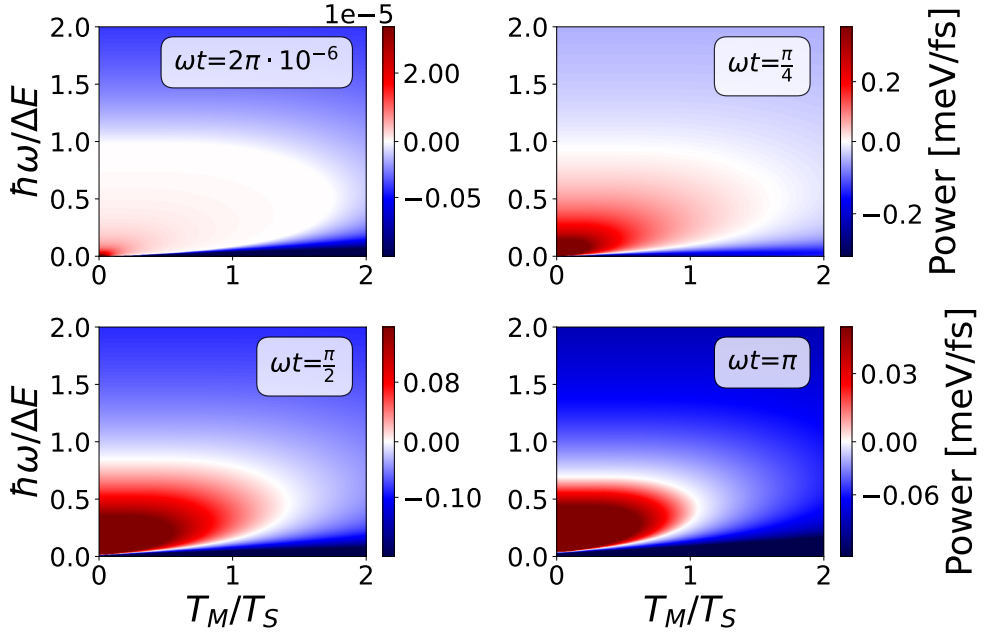

Figure 4.4: Heatmap of power generation relying on $W_\mathrm{ext}^\mathrm{exc}$ at four different times, $\tau = 10^{-6}$ to approximate the Zeno limit and the rest chosen linearly spaced between 0 and $\tau = 0.5$.

Common for both the case when using excess work in Fig. 4.4, and when using ergotropy in Fig. 4.5, is that there is low power in the short time limit. Other common features between the two cases are that low relative energy spacings and low relative temperatures are preferred. Two clear differences arise in the case of excess work compared to ergotropy. The first difference is that there is a smooth boundary for the positive power producing region in Fig. 4.4, whereas there is a fan-like behaviour in Fig. 4.5. This fan-like behaviour arises due to the ergotropy itself, as can be seen in Fig. 4.6, where only the ergotropy is shown, whereas Fig. 4.5 shows the ergotropy minus the measurement work. Fig. 4.6 shows the ergotropy using the same parameters, and at the same times as all the other heatmaps presented here, the white areas correspond to the regions where the ergotropy is exactly zero. The second difference is that, despite using the same parameter set, the temperature range in which the two definitions of work produce net positive power is drastically different. Specifically, in Fig. 4.4 positive power can be extracted even for $T_\mathrm{M}/T_\mathrm{S} > 1$ whereas in Fig. 4.5 positive power is only extracted up to $T_\mathrm{M}/T_\mathrm{S} \approx 0.5$.

Figure 4.6 is essentially similar to Fig. 4.5, however, without subtracting the measurement work. That is, in this case $\Pi = \frac{W_\mathrm{ext}}{t_\mathrm{m}}$. It is presented here to more

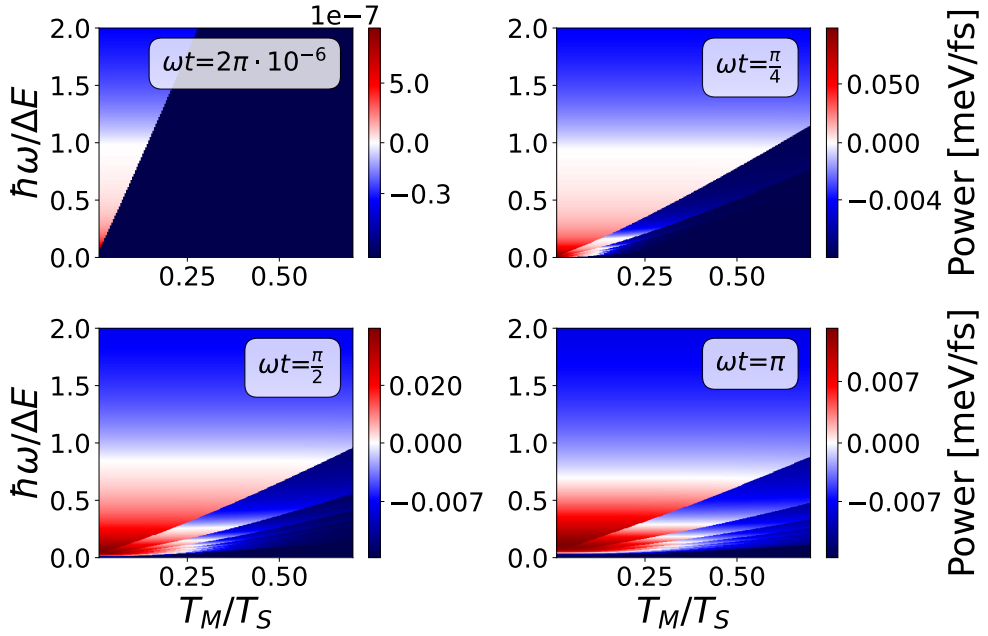

Figure 4.5: Heatmap of power generation relying in $W_{\text{ext}}^{\text{erg}}$ at four different times for different ratios of temperature and different ratios of $\frac{\hbar\omega}{\Delta E}$.

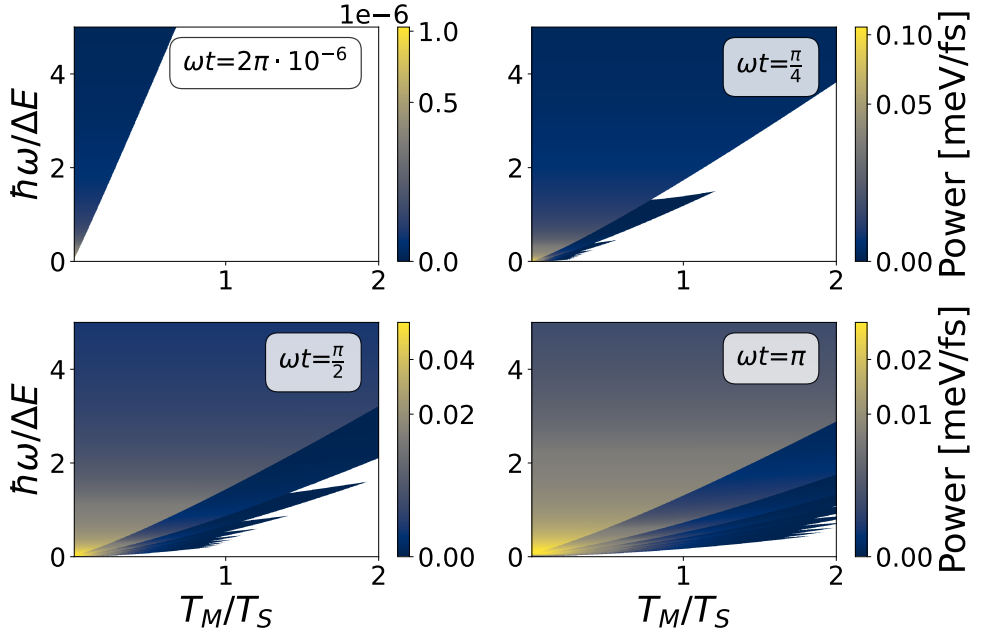

Figure 4.6: Heatmap of the ergotropy at four different times and for different ratios of temperatures and $\frac{\hbar\omega_0}{\Delta E}$. The white region corresponds to the ergotropy being exactly zero, this is done to highlight the fan-like behaviour of the ergotropy.

clearly show the origin of the fan-like behaviour of Fig. 4.5.

Only the heat maps corresponding to the dissipative evolution are presented

here, because measurement times have been kept short and the coupling between the meter and the bath is weak, hence the difference to the unitary evolution is negligible.

4.3.2 Discussion: Temperature and Energy Spacing Effects

Within the heat maps of ergotropy and net power generation shown in Figs. 4.5 and 4.6, a notable aspect is the striations apparent in the former and the jagged boundary present in the latter. The jagged edges in the boundary of positive and negative net power production correspond to the striations in the ergotropy, so the underlying cause is the behaviour of the ergotropy. Although a definitive cause for these striations is unknown, a plausible hypothesis is the discrete nature of the activation threshold n'. According to Eq. (3.44), the summation begins at n', where n' is the minimal n that satisfies $P(1|n, t_\mathrm{m}) > P(0|n, t_\mathrm{m})$. For certain n' and initial temperature T'_M, as T_M increases, there is a likelihood of reaching a point where this condition fails, requiring the summation to start from $n' + 1$. These discrete transitions might be the reason behind this observed behaviour. A comparison may be made with excess work, where the activation threshold n' is fixed from the outside rather than updated dynamically, which shows no discrete steps unlike ergotropy.

Apart from the above features, other noteworthy features are that regardless of whether excess work or ergotropy is used as a measure of the extracted work, there seems to be a preference for relatively cold meters, with relatively small energy spacings. This makes sense, as with a relatively cold meter the thermal population will be concentrated in the lower eigenstates of the QHO and any changes in the meter population due to coupling with the system should be more apparent. Similarly, with a smaller energy spacing, even relatively small effects from the coupling to the system should be able to affect the population distribution of the meter. In short, a colder meter yields less thermal noise, and a smaller energy spacing allows a more fine-grained measurement. Then it seems that the temperature of the meter is a critical limitation for the extraction of work; excessive temperature leads to noise saturation, which affects the gathering of information, rendering the IE non-functional. However, a low temperature of the meter does not necessarily imply a low ratio of $\frac{T_\mathrm{M}}{T_\mathrm{S}}$, which seems to be the limiting factor in Figs. 4.4 and 4.5. For instance, we might imagine a transmon qubit coupled to a waveguide resonator that would both be held at cryogenic temperatures in a dilution fridge. This would result in a temperature ratio of 1, while simultaneously reducing the likelihood of thermal noise saturating the meter.

Assuming that $\hbar\omega$ and T_M remain constant at values conducive to effective information readout, how can we improve engine work output? Several factors are at play, and I restrict the discussion to using ergotropy as a measure of work. First, we recall Eq. (3.44) and note that the ergotropy depends both on the energy splitting of the TLS, ΔE, and on the difference in the joint probabilities, $P(1, n, t_\mathrm{m}) - P(0, n, t_\mathrm{m})$. Now, $P(0, n, t_\mathrm{m}) \propto a$ and $P(1, n, t_\mathrm{m}) \propto b$ where a, b are the initial ground- and excited-state populations of TLS. Naively, increasing ΔE would lead to more energy extracted per successful extraction attempt and therefore could lead to a higher work output. However, $b \to \infty$ as $\Delta E \to \infty$ meaning that an infinitely high energy

splitting means the TLS never reaches the excited state and no work can be extracted, thus it seems that simply increasing ΔE is not the solution. Similarly, we may consider raising b by allowing $T_S \to \infty$; however, since $W_{\text{meas}} \propto b$, increasing b also maximises the measurement work. Then a solution would be to increase both ΔE and T_S so that b remains constant at an appropriate value. Increasing these two parameters together would also decrease the ratios $\frac{\hbar\omega}{\Delta E}$ and $\frac{T_M}{T_S}$ together, explaining the behaviour seen in Fig. 4.5 where a low temperature *ratio* is preferred, not just a low temperature.

4.3.3 Influence of Coupling Strength

Figures 4.7 and 4.9 show heat maps similar to those discussed in Sections 4.3.1 and 4.3.2 where again the x-axis shows the temperature ratio $\frac{T_M}{T_S}$; however, the y-axis is now the ratio of the effective coupling strength squared, $g_{eff}^2 = g^2 M$, to the energy splitting of the TLS, ΔE. The same four distinct times are chosen, and again the red region corresponds to positive power output, and the blue region to negative power output. A notable feature is the scaling of power to coupling strength in the approximate Zeno limit case; here it seems that a higher coupling strength is always preferred, whereas for longer times this is not the case.

Examining the power output as a function of the ratio between the energy splitting of the system and the strength of the coupling between the system and the meter may serve as a useful guide in designing future experiments. This is shown in Fig. 4.9 for the excessive work engine and in Fig. 4.7 for the ergotropic engine. Once again we see in both of these images a tendency for the power production in the Zeno limit to become very low. In fact, in Fig. 4.7, as in Fig. 4.5, the approximate Zeno limit results in low power and a relatively small viable parameter regime. Figure 4.8 shows the ergotropy as a function of temperature and effective coupling strength. Notable here is that the slight oscillatory behaviour shown in Fig. 4.8 appears to have been washed out in Fig. 4.7.

4.3.4 Discussion: Influence of Coupling Strength

Just as in Fig. 4.6, there appears to be some oscillating behaviour present in Fig. 4.8. However, this behaviour does not appear to be present when looking at the net power output, that is, when subtracting the measurement work, in Fig. 4.7, and the cause of this is unknown. However, since the net work in this case is simply $W_{\text{ext}}^{\text{erg}} - W_{\text{meas}}$ a possible explanation is that the resolution of the graph is too low and that with more fine-grained data, looking at a smaller area, these oscillations would appear again. Regardless, the data shown in Figs. 4.7 and 4.8 is essentially the same, it comes from the same simulation and the only difference in the graphs is the subtraction of the measurement work, i.e. one graph shows $\frac{W_{\text{ext}}^{\text{erg}} - W_{\text{meas}}}{t_m}$ and the other shows $\frac{W_{\text{ext}}^{\text{erg}}}{t_m}$. The conclusion is that both the wash-out of the oscillations on the boundary, and the change in shape is entirely due to the influence of the measurement work.

An important aspect for finite times is that an "intermediate" coupling strength is preferable. With zero coupling strength, no work is extracted, as anticipated, because the system and meter lack correlation. The lack of correlation means that

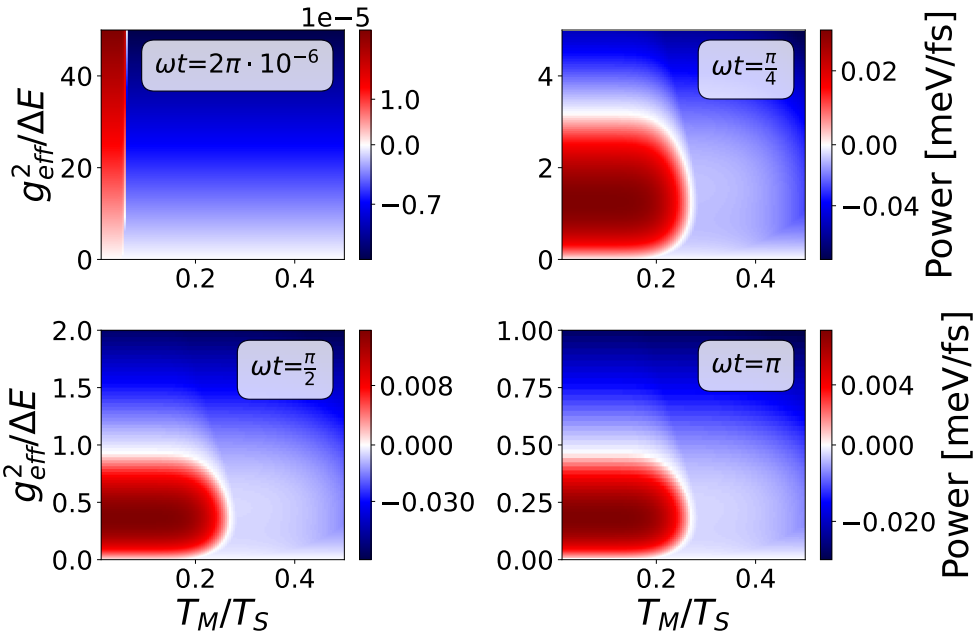

Figure 4.7: Heatmap of power generation relying on $W_{\text{ext}}^{\text{erg}}$ at four different times. The x-axis shows the ratio of temperatures T_{M} and T_{S}, and the y-axis shows the ratio of the effective coupling strength g_{eff}^2 to the energy splitting of the system, ΔE.

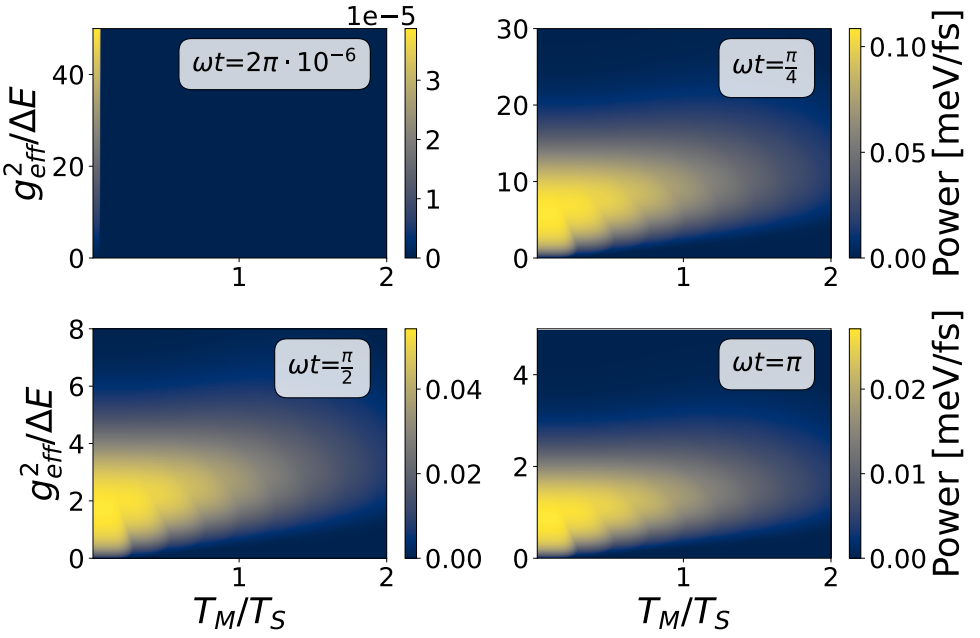

Figure 4.8: Heatmap of the ergotropy at four different times. The x-axis shows the ratio of temperatures T_{M} and T_{S}, and the y-axis shows the ratio of the effective coupling strength g_{eff}^2 to the energy splitting of the system, ΔE.

any attempt to extract work is no better than a random guess, and thus no work

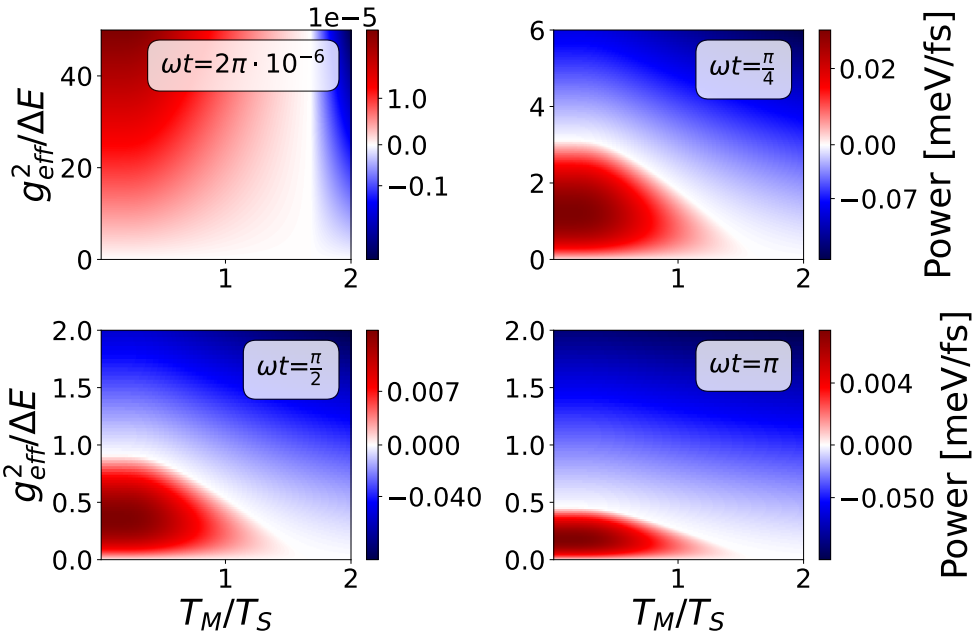

Figure 4.9: Heatmap of power generation relying on $W_{\text{ext}}^{\text{exc}}$ at four different times. The x-axis shows the ratio of temperatures T_{M} and T_{S}, and the y-axis shows the ratio of the effective coupling strength g_{eff}^2 to the energy splitting of the system, ΔE.

is extracted. Similarly, for high coupling strengths and finite times, the power output becomes negative because the measurement work scales with the square of the effective coupling strength. This does not happen in the short time limit, because in the short time limit the measurement work also scales with t_{m}^2 where t_{m} is the measurement time.

Finally, it seems that the net power producing regions in Section 4.3.3 and Fig. 4.7 increase in size with small to intermediate ratios of $\frac{g_{eff}^2}{\Delta E}$. This could, hopefully, serve as a guide in choosing experimental parameters in the future.

4.4 Engine Efficiency: Excess Work vs. Ergotropy

The efficiencies of the engine for the two different cases of extracted work are shown in Fig. 4.10 where (a) uses the excess work to define the extracted work and (b) uses the ergotropy. Notable is the fact that the efficiency of the ergotropic engine is always bounded by both the Carnot and CNCA efficiencies. However, the excessive work engine manages not only to produce work in the $T_{\text{M}} > T_{\text{S}}$ regime, but also to *seemingly* exceed both the Carnot and the Chambadal-Novikov-Curzon-Ahlborn (CNCA) efficiencies. It is appropriate to exercise caution with regard to a result such as this, and a discussion is offered in Section 4.4.1.

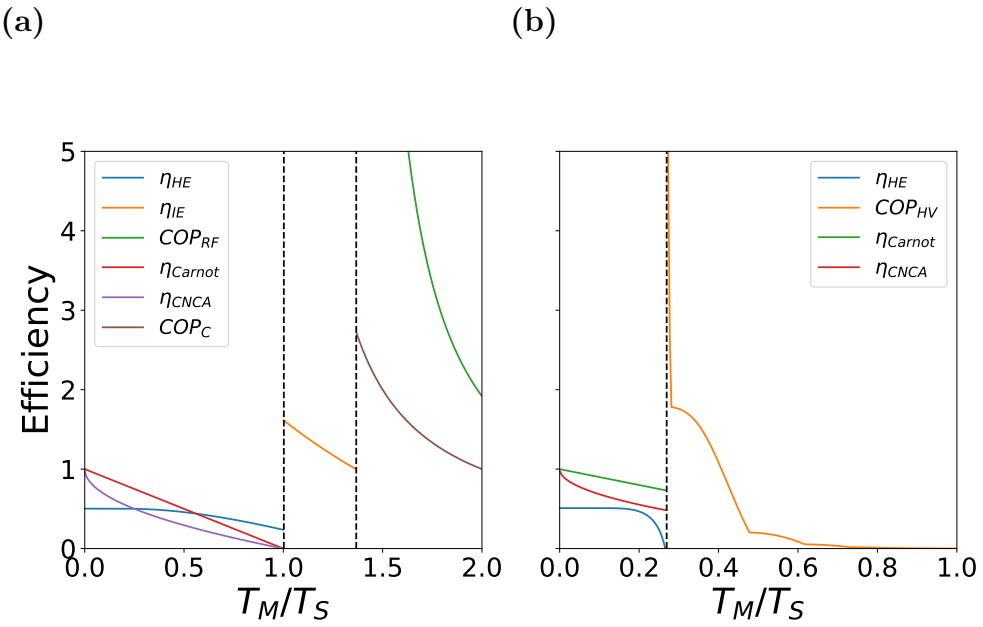

Figure 4.10: Efficiency of the engine when th extracted work is defined using (a) excess work, and (b) using ergotropy. Note that the temperature ranges are different since the use of ergotropy never allows the engine to produce work at $\frac{T_\mathrm{M}}{T_\mathrm{S}} > 1$. The Carnot bounds η_Carnot, COP_C, and the CNCA bound η_CNCA are included for reference.

4.4.1 Discussion of Engine Efficiency

Returning briefly to the efficiency graph shown in Fig. 4.10(b), it is notable that the efficiency, when assuming that the engine extracts the ergotropy, is bounded by both the Carnot and the CNCA efficiencies. The efficiency of the QIE approaches, but never equals, the CNCA efficiency. It is unknown whether this is a matter of parameters; perhaps, through some optimisation process, a measurement time might be chosen such that η_{HE} coincides with η_{CNCA}. As ergotropy represents the maximum work that can be extracted under unitary transformations, it seems likely that such a measurement time should exist or at least that η_{CNCA} should be attainable through some combination of parameters.

As for the efficiency shown in Section 3.5(a), the efficiency of the QIE *appears* to exceed the Carnot efficiency. To be clear, I do not make the claim that the efficiency actually exceeds the Carnot efficiency. Rather, this suggests that some energy cost is not properly accounted for, or that perhaps the definition of efficiency given in Eq. (3.69) is not suitable in the context of extraction of work through a dissipative channel as in this case. Consider, for instance, Fig. 4.11 which shows the conditional probabilities of being to the ground or excited states at some time t given a measurement outcome n in the Fock basis of the QHO. The solid blue

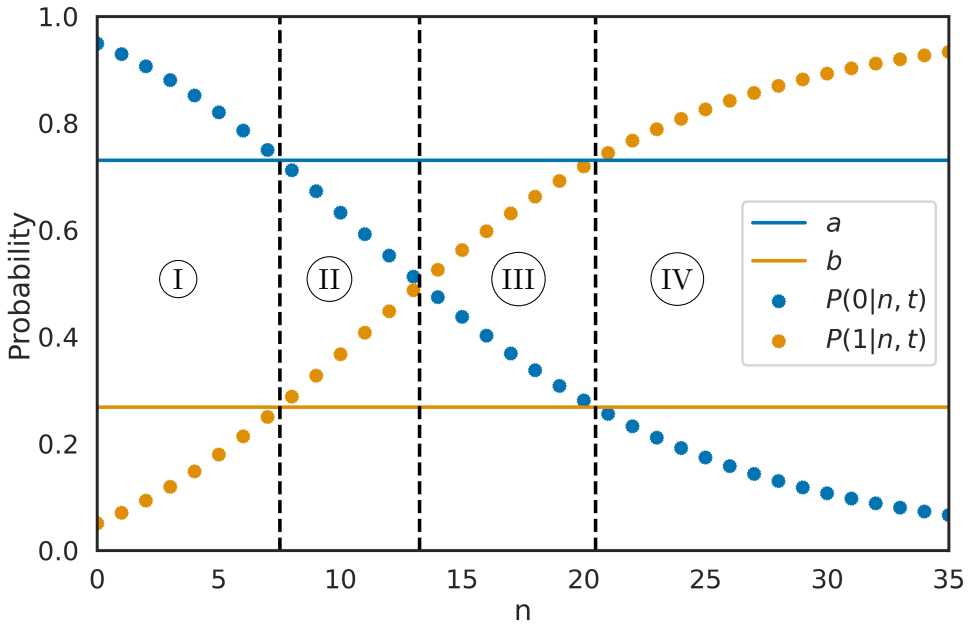

Figure 4.11: The figure shows the conditional probabilities for the TLS to be in the excited state, given that we measure the QHO to be in state n. The solid lines show the initial state where a and b are the initial populations in the ground state and excited state, respectively. The dotted lines show the evolution of the conditional probabilities as the meter is populated in increasingly energetic states. The dashed vertical lines show where the conditional probabilities cross the initial state populations, and where they cross each other.

and orange lines in the graph are the initial populations of the states $|0\rangle$ and $|1\rangle$,

respectively, while the dotted lines are the conditional probabilities after the meter and the system have been allowed to correlate for some time t. As expected, the initial state is passive. The graph can be divided into four sections, I - IV, from left to right. In region I the state is passive even after measurement, and no work can be extracted. In region IV the system is in an active state, and regardless of the definition of extracted work, there is no problem here. Work is extracted via population inversion, basically by performing some unitary transformation that swaps the place of the dotted blue and orange lines and then paying some amount of work to rethermalise back to the initial populations. In essence, this is the idea of ergotropy, with the penalty of rethermalising back to the initial state. The ambiguity around the definition of excess work arises in regions II and III. In region III the idea is similar to that in region IV, except that this time we extract work in the process of rethermalizing back to the initial state. Conversely, region II does not support any population inversion, as it is in a passive state. Nevertheless, it appears to permit the extraction of work by rethermalising to the original state. That is, we could imagine taking the system, connecting it to a bath of temperature T_{S} and inserting a heat engine between the two in order to extract work as the system rethermalises to T_{S}. When ergotropy is utilised as a metric for extracted work, regions III and IV are the only ones where work can be extracted, as it relies exclusively on population inversion. This might go some way to explaining the different behaviours of excess work and ergotropy.

5
Conclusion

In conclusion, this thesis has considered a QIE using a TLS as the working medium and a QHO as the meter. The role of measurement time, in this case the time during which the working medium and the meter are allowed to correlate, has been examined. The general conclusion is that for finite power production, we require finite measurement times and that the measurement time is an important parameter to consider in setups like the one considered in this thesis. While the short-time limit, or Zeno limit, may give some physical intuition on how the system behaves, it may not be the best choice in operating the engine. At least not if high power is desired for each individual cycle of the engine.

Two different metrics for the extracted work are also considered, excess work and ergotropy. In both cases a condition for net positive work output was found for the short-time limit. It is also worth noting that the excess work, as previously shown and discussed, seems to be non-unitary in some way. In particular, the activation threshold n' is set from the outside, and how this would be done in an experimentally realisable manner is unclear. The ergotropy, on the other hand, merely presents a bound on the work that can be extracted, and it is unlikely that we actually reach this in an experiment. It is my opinion that both of these metrics could be useful when evaluating IEs with the caveat that one must be cognizant of their limitations, ergotropy is limited to unitary transformations and, conversely, excess work appears to be nonunitary. It is particularly important to meticulously evaluate the definition of efficiency when dealing with excess work and relating it to established outcomes, such as the Carnot efficiency, to ensure that comparisons are made in a consistent manner. Failing to do so might lead to outcomes as in Fig. 4.10 (a), where the efficiency *seems to* exceed Carnot. Thus, it appears that the chosen work metric, be it ergotropy or excess work, fundamentally alters the perceived performance and thermodynamic consistency of the engine.

The discrete nature of the meter seems to result in a complex, oscillatory, behaviour of the ergotropy, and this may warrant further investigation. In particular, it is interesting that the oscillatory behaviour in Fig. 4.8 vanishes in Fig. 4.7.

There seems to be a preference for the measurement device, the QHO, to be relatively cold and have a small energy spacing $\hbar\omega$ as discussed in Section 4.3.2. There also seems to be a preference for a small to intermediate-sized coupling strength, as discussed in Section 4.3.4, and hopefully these results may serve as guidelines in designing potential future experiments.

5.1 Summary

In summary, this thesis has considered the energetic cost of quantum measurement and the related information acquisition in finite-time operations. The main results are

- A general condition for positive work extraction in the Zeno limit has been found in Eqs. (3.65) and (3.68).
- As the measurement time approaches zero, so does the extracted work.
- Ergotropy, while itself a highly idealised process, might be a more physical definition of the extracted work in a QIE cycle, compared to excess work.
- The discreteness of the meter, in particular, influences the behaviour of the engine producing discrete steps in the region admitting positive power production.
- There are nontrivial trade-offs to consider when designing the system and meter parameters, and this thesis may serve as a guide for how these parameters should be chosen.

5.2 Outlook

This thesis has focused on average quantities produced over many engine cycles. However, in nanoscale devices fluctuations play an important role [48] and it's yet unclear how the performance of this QIE might change when taking fluctuations into account.

A further aspect to investigate is the effect finite temperatures for the demon, or the classical memory. The temperature of the Maxwell demon, T_D is an additional degree of freedom in the system and in this work, and in others [34], T_D is set to zero in order to dump entropy into a zero-temperature bath thus fulfilling the second law of thermodynamics without the creation of additional heat. However, there is no one single way to choose T_D but rather it may depend upon the particular implementation of the QIE. It's clear that no such thing as a zero-temperature bath truly exists, and for that reason further investigating the effects of finite demon temperatures would be interesting.

Moreover, it becomes clear that while studying dimensionless parameters, e.g. $\frac{T_M}{T_S}$ or $\frac{\hbar\omega_0}{\Delta E}$, can reduce the effective number of parameters in the system there are still many parameters to consider when designing a QIE. While this thesis can hopefully provide some guidance in the choice of parameters a more thorough result might be found by studying Pareto fronts to obtain a reduced set of Pareto-optimal parameters.

In discussions with an experimental group it has been suggested that a more suitable formulation of the problem, at least given their experimental setups, would be to measure $\hat{x}$ rather than measuring in the Fock basis. Reformulating the problem this way should be doable but it's unclear what complications, if any, this might bring.

Finally, there is always a trade-off between measurement, available resources, and noise. In particular, the creation of a pure state requires a diverging amount of resources [19]. This aspect has been neglected in the analysis presented in the thesis. A relevant question to consider is the loss of measurement precision under the constraint of finit time and finite energy, and what impact this would have on the performance of the QIE.

Bibliography

1. Saslow, W. M. A History of Thermodynamics: The Missing Manual. *Entropy* **22,** 77. ISSN: 10994300. https://pmc.ncbi.nlm.nih.gov/articles/PMC7516509/ (Jan. 2020).
2. Schroeder, D. V. *An Introduction to Thermal Physics* (2000).
3. Knott, C. G. *Life and Scientific Work of Peter Guthrie Tait* 213–215 (Cambridge University Press, 1911).
4. THOMSON, W. Kinetic Theory of the Dissipation of Energy. *Nature* **9,** 441–444. ISSN: 1476-4687. https://doi.org/10.1038/009441c0 (1874).
5. Szilard, L. über die Entropieverminderung in einem thermodynamischen System bei Eingriffen intelligenter Wesen. *Zeitschrift für Physik* **53,** 840–856. ISSN: 0044-3328. https://doi.org/10.1007/BF01341281 (1929).
6. Brillouin, L. Maxwell's demon cannot operate: Information and entropy. I. *Journal of Applied Physics* **22,** 334–337. ISSN: 00218979 (1951).
7. Landauer, R. Irreversibility and Heat Generation in the Computing Process. *IBM Journal of Research and Development* **5,** 183–191. ISSN: 0018-8646 VO - 5 (1961).
8. Bennett, C. H. The Thermodynamics of Computation–a Review. *International Journal of Theoretical Physics* **21,** 905–940 (1982).
9. Auffèves, A. Quantum Technologies Need a Quantum Energy Initiative. *PRX Quantum* **3,** 1. ISSN: 26913399. https://doi.org/10.1103/PRXQuantum.3.020101 (2022).
10. Sagawa, T. & Ueda, M. Second law of thermodynamics with discrete quantum feedback control. *Physical Review Letters* **100.** ISSN: 00319007 (2008).
11. Toyabe, S., Sagawa, T., Ueda, M., Muneyuki, E. & Sano, M. Experimental demonstration of information-to-energy conversion and validation of the generalized Jarzynski equality. *Nature Physics 2010 6:12* **6,** 988–992. ISSN: 1745-2481. https://www.nature.com/articles/nphys1821 (Nov. 2010).
12. Koski, J. V., Maisi, V. F., Pekola, J. P. & Averin, D. V. Experimental realization of a Szilard engine with a single electron. *Proceedings of the National Academy of Sciences* **111,** 13786–13789. https://doi.org/10.1073/pnas.1406966111 (Sept. 2014).

13. Elouard, C. & Jordan, A. N. Efficient Quantum Measurement Engines. *Physical Review Letters* **120.** ISSN: 1079-7114. https://doi.org/10.1103/PhysRevLett.120.260601 (2018).

14. Bresque, L. *et al.* Two-Qubit Engine Fueled by Entanglement and Local Measurements. *Physical Review Letters* **126,** 1–6. ISSN: 10797114 (2021).

15. Kirchberg, H. & Nitzan, A. *Quantum Information Engines : Assessing Time , Cost and Performance Criteria* 2024. https://arxiv.org/abs/2404.17431.

16. Zurek, W. H. Decoherence and the transition from quantum to classical - Revisited. *Progress in Mathematical Physics* **48,** 1–31. ISSN: 15449998 (2007).

17. Von Neumann, J. *Mathematische Grundlagen der Quantenmechanik* **4** (Springer, Berlin, 1932).

18. Hance, J. R. & Hossenfelder, S. What does it take to solve the measurement problem? *Journal of Physics Communications* **6.** ISSN: 23996528 (2022).

19. Taranto, P. *et al.* Landauer Versus Nernst: What is the True Cost of Cooling a Quantum System?

20. Griffiths, D. J. . & Schroeter, D. F. *Introduction to Quantum Mechanics* 3rd ed. ISBN: 978-1-107-18963-8 (Cambridge University Press, Cambridge, United Kingdom, 2018).

21. Sakurai, J. J. & Napolitano, J. *Modern Quantum Mechanics* 3rd ed. (Cambridge University Press, 2020).

22. Breuer, H.-P. & Petruccione, F. *The Theory of Open Quantum Systems* Jan. 2007. https://doi.org/10.1093/acprof:oso/9780199213900.001.0001.

23. Nielsen, M. A. & Chuang, I. L. *Quantum Computation and Quantum Information* 10th Anniv. ISBN: 978-1-107-00217-3 (Cambridge University Press, Cambridge, United Kingdom, 2010).

24. Landi, G. T. *Quantum information and quantum noise* 2018.

25. Lindblad, G. On the generators of quantum dynamical semigroups. *Communications in Mathematical Physics* **48,** 119–130. ISSN: 1432-0916. https://doi.org/10.1007/BF01608499 (1976).

26. Gorini, V., Kossakowski, A. & Sudarshan, E. C. G. Completely positive dynamical semigroups of N-level systems. *Journal of Mathematical Physics* **17,** 821–825. ISSN: 0022-2488. https://doi.org/10.1063/1.522979 (May 1976).

27. Potts, P. P. in *Lecture notes* 89–115 (2022). https://link.springer.com/10.1007/978-981-16-6644-5_8.

28. Sethna, J. P. *Statistical Mechanics: Entropy, Order Parameters, and Complexity* ISBN: 9780198865247. https://doi.org/10.1093/oso/9780198865247.001.0001 (Oxford University Press, 2021).

29. Shannon, C. E. A mathematical theory of communication. *The Bell System Technical Journal* **27,** 379–423. ISSN: 0005-8580 VO - 27 (1948).

30. MacKay, D. J. C. *Information Theory, Inference, and Learning Algorithms* 7.2. ISBN: 0521642981 (Cambridge University Press, 2005).

31. Curzon, F. L. & Ahlborn, B. Efficiency of a Carnot engine at maximum power output. *American Journal of Physics* **43,** 22–24. ISSN: 0002-9505 (1975).

32. Chambadal, P. *Les centrales nucléaires* https://books.google.se/books?id=TX8KAAAAMAAJ (A. Colin, 1957).

33. Kim, S. W., Sagawa, T., De Liberato, S. & Ueda, M. Quantum Szilard Engine. *Physical Review Letters* **106,** 1–4. ISSN: 00319007 (2011).

34. Dassonneville, R. *et al.* Directly probing work extraction from a single qubit engine fueled by quantum measurements, 1–12. http://arxiv.org/abs/2501.17069 (2025).

35. Cahill, K. E. & Glauber, R. J. Ordered Expansions in Boson Amplitude Operatos. *Physical Review* **177** (1969).

36. Magnus, W., Oberhettinger, F. & Soni, R. P. *Formulas and Theorems for the Special Functions of Mathematical Physics* 239–249. ISBN: 9783662117637 (1966).

37. Virtanen, P. *et al.* {SciPy} 1.0: Fundamental Algorithms for Scientific Computing in Python. *Nature Methods* **17,** 261–272 (2020).

38. Allahverdyan, A. E., Balian, R. & Nieuwenhuizen, T. M. Maximal work extraction from finite quantum systems. *Europhysics Letters* **67,** 565–571. ISSN: 02955075 (2004).

39. Francica, G., Goold, J., Plastina, F. & Paternostro, M. Daemonic ergotropy: Enhanced work extraction from quantum correlations. *npj Quantum Information* **3,** 1–5. ISSN: 20566387. http://dx.doi.org/10.1038/s41534-017-0012-8 (2017).

40. Misra, B. & Sudarshan, E. C. The Zeno's paradox in quantum theory. *Journal of Mathematical Physics* **18,** 756–763. ISSN: 00222488 (1977).

41. Facchi, P. & Pascazio, S. Quantum Zeno dynamics: Mathematical and physical aspects. *Journal of Physics A: Mathematical and Theoretical* **41.** ISSN: 17518113 (2008).

42. Van Rossum, G. & Drake, F. L. *Python 3 Reference Manual* ISBN: 1441412697 (CreateSpace, Scotts Valley, CA, 2009).

43. Harris, C. R. *et al.* Array programming with {NumPy}. *Nature* **585,** 357–362. https://doi.org/10.1038/s41586-020-2649-2 (Sept. 2020).

44. Hunter, J. D. Matplotlib: A 2D graphics environment. *Computing in Science & Engineering* **9,** 90–95 (2007).

45. Waskom, M. L. seaborn: statistical data visualization. *Journal of Open Source Software* **6,** 3021. https://doi.org/10.21105/joss.03021 (2021).

46. Golyshev, V. Y. The dynamics of a quantum harmonic oscillator in a dissipative environment. *Technical Physics Letters* **28,** 61–63. ISSN: 1090-6533. https://doi.org/10.1134/1.1448645 (2002).

47. Di Bello, G. *et al.* Qubit-oscillator relationships in the open quantum Rabi model: the role of dissipation. *The European Physical Journal Plus* **138,** 135. ISSN: 2190-5444. https://doi.org/10.1140/epjp/s13360-023-03714-x (2023).

48. Palmqvist, D. Bounds on entropy production and its noise in bosonic systems Thermodynamic constraints on noise in the coherent transport (2024).

DEPARTMENT OF MICROTECHNOLOGY AND NANOSCIENCE
CHALMERS UNIVERSITY OF TECHNOLOGY
Gothenburg, Sweden
www.chalmers.se

CHALMERS
UNIVERSITY OF TECHNOLOGY